THE EXPERIMENTAL DETERMINATION OF ROTOR BLADE DYNAMIC BENDING MOMENTS OF A 10-kW WIND TURBINE

by

David Gerard Hendricks

Thesis submitted to the Faculty of the
Virginia Polytechnic Institute and State University
in partial fulfillment of the requirements for the degree of
MASTER OF SCIENCE
in
Mechanical Engineering

APPROVED:

H. L. Moses, Chairman

W. F. O'Brien

D. H. Vaughan

May, 1991

Blacksburg, VA

THE EXPERIMENTAL DETERMINATION OF ROTOR BLADE DYNAMIC BENDING MOMENTS OF A 10-kW WIND TURBINE

by

David Gerard Hendricks

Committee Chairman: Hal L. Moses
Mechanical Engineering

(ABSTRACT)

A 10-kW horizontal axis wind turbine was studied to determine the effects of wind shear and gravity on rotor blade bending moments.

A drag sphere based wind measuring system was designed to measure rapid fluctuations in wind velocity at two different heights. However, severe power line noise problems with the low level signals forced the use of standard rotating cup anemometry.

Rotor blade bending moments were obtained with strain gages mounted on blade extenders near the root of the instrumented blade. Rotor angular position data were obtained with a photocell arrangement.

The one per revolution primary bending moment frequency was caused mostly by gravity-induced bending. Also present is the 6 Hz blade natural frequency.

A logarithmic atmospheric boundary layer (ABL) profile was used to estimate wind conditions at the upper level. Examination of the bending moment data revealed good agreement with values predicted from the ABL profile (within 4% in the mean) indicating the profile was a good mean approximation.

ACKNOWLEDGEMENTS

The author would like to extend many thanks to his major professor, Dr. Hal Moses, and the other members of his advisory committee, namely Dr. Walter O'Brien and Dr. David Vaughan, for their guidance and wisdom in the preparation and completion of this thesis.

Thanks to the guys in the Mechanical Engineering Shop, especially Johnny Cox, Frank Caldwell, and Billy Shepherd, for all of their knowledge and help in explaining things to me and getting the job done. Also, I would like to thank the Virginia Tech Electric Service for providing the equipment and support in erecting the turbine and tower.

My parents get a special note of thanks for their love, support, and advice the whole way through. They have always been there to get me through the tough times in my life, and this was definitely no exception.

Last, but by no means least, there is Cheryl. She was forever giving me love and a promise for better days to get me through the hard times. Without her love and encouragement, completion of this work would have been extremely difficult.

TABLE OF CONTENTS

LIST OF FIGURES

LIST OF TABLES

CHAPTER 1 – INTRODUCTION

Many studies have been done over the years concerning the performance aspects of wind turbines. Thorough analyses of such things as power output, lift and drag of the blades, and efficiency provide much useful information and guidance. However, only limited data are available concerning the effects of fluctuating wind speeds and wind shear on the bending moments in the wind turbine blades. Wind shear is that condition resulting from unequal wind speeds at different heights, usually due to the atmospheric boundary layer (ABL). Such information would be helpful in determining the results of utilizing sites with radical wind shear characteristics in future wind turbine applications.

There are a great many aspects related to a wind speed versus blade stress analysis that can be researched. The mean and maximum stresses can be correlated with wind speed, frequency analyses in the form of Fast Fourier Transforms (FFT's) or autoregressive (AR) modelling techniques can be performed to determine critical harmonics, and detailed fatigue analyses can be accomplished via so-called "rainflow" procedures to

quantify the fatigue life of the blades. The wind turbine in question has already had the first set of work completed, namely the basic blade stress versus wind speed experiment. The scope of this thesis is to perform a refined version of the above-mentioned experiment.

The accounting of wind shear effects on the blade loads is a major concern in the design of large wind turbines. A brief discussion of this topic is of interest here as the determination of this effect constitutes one focus of this thesis.

For the purposes of this thesis wind shear is defined as the difference in wind speed due to a change in altitude. A increase in wind speed will result from a increase in height due to the ABL. For any given rotor speed this means an increase in the relative incoming velocity of air to the rotor between the upper and lower portions of the blade circle. Thus, the angle of attack will also increase. This results in subsequent increases in lift (that force perpendicular to the relative velocity) and drag (that force parallel to the relative velocity). The resultant of these two forces is perpendicular to the blade chord and causes the blade bending moment. Thus, the bending moment will increase as the blade travels upward.

The wind turbine being studied is an upwind 10-kW horizontal axis type built by the Elektro Company of Switzerland. It is mounted atop a 20 ft (6.1 m) tower. The blades are kept facing into the wind and turned out of the wind by way of a pivoting tail section. The site is located approximately 7 miles (11 km) northwest of Newport, Virginia in the Alleghany Mountains. The parameters being studied with this turbine setup include the wind-induced as well as gravity-induced bending moments in one of the blades. A detailed study of wind shear effects on the bending moment was originally intended to be explored, but severe power line noise problems in the wind measuring system prohibited an in-depth examination of these effects.

This thesis is divided into five chapters. Figures and Tables are presented at the end of the chapter in which they are introduced. Chapter 2 gives a brief historical account of windmills, followed by a technical review of not only previous studies of this particular wind turbine, but also some industry research efforts in wind turbine optimization. A discussion of wind shear effects on blade bending moments is also included. Chapter 3 provides a detailed description of the apparatus used in the accomplishment of the experiment. Though the majority of the equipment was not built or modified by the author, an

understanding of their operation was essential and is given as a reference to those who may operate and analyze this wind turbine in the future. The concepts and design procedures of the equipment designed, built, and tested by the author are also presented. Chapter 4 presents the data and results of the wind shear analysis and blade bending moment comparison. Figures showing the relationships between blade bending moment and wind speed are given. A discussion of the experiment is included. Chapter 5 lists the conclusions gleaned from the work accomplished and also suggests recommendations for not only how this project could have been improved, but also what further work may be of use in the future.

CHAPTER 2 – LITERATURE REVIEW

HISTORICAL BACKGROUND: The development of wind power is a continuously changing field. New advances and updates in the state-of-the-art allow larger, more powerful, and more aerodynamically efficient wind energy conversion systems (WECS) to be introduced. The advances in WECS technology may one day allow wind energy to be a viable option on a large scale. This is especially important with the so-called "greenhouse effect" seemingly becoming a reality partly through the worldwide burning of fossil fuels. To help understand how the present state of the art arose, a brief review of wind turbine development follows.

Clarification should be made at this point to distinguish between wind "turbines" and wind "mills". The former is used to identify those machines which convert wind energy into electrical energy. Windmills, on the other hand, are used to convert wind energy into mechanical work in order to power a grinding mill or some similar operation. Since windmills came first chronologically the term is still used by many people today in reference to wind turbines, though obviously a misnomer exists. For clarity, the comprehensive term "wind machine" will be used when both wind turbines and windmills apply.

Wind turbines can be classified as one of two basic types: vertical axis wind turbines (VAWT's) or horizontal axis wind turbines (HAWT's). Figure 2.1 shows the basic arrangement of each type. The earliest machines were of a VAWT design. Although the Chinese were known to take advantage of wind power as early as 2000 B.C., credit is generally given to the Persians around the fourth or fifth century B.C. for the first widespread utilization of wind power [2]. A typical Persian windmill is shown in Figure 2.2. Obviously a VAWT design, the rotor's vertical axis spins a millstone at the base of the structure to grind grain against the bedstone.

Some claim that windmills found their way into Europe after the Crusaders returned from the Middle East, though VAWT type machines were not found in any great numbers in Europe. Necessity and advancements in technology led to windmills of the HAWT type there. At first the only use of windmills in Europe was, as in Asia, the processing of grain. However, as the Dutch began to reclaim flooded lands for agriculture and settlement, the role of pump-driver became a much used function.

The majority of European windmills were the post mills, first used in Germany in the thirteenth century [3].

A typical mill consisted of a HAWT type machine whose supporting tower is mounted on a post so that the sails could be turned to face into the wind when needed. The Dutch improved upon this concept with the smock, or tower, mill, which is basically a post mill with only the topmost portion rotatable as shown in Figure 2.3. At first the mills were turned manually, either by human or animal strength. It was the smock mills that allowed the Dutch to drain vast quantities of flooded land.

Eventually the process of manually rotating the mills grew quite tiresome, due to both labor requirements and the slow response to wind conditions. The fantail, patented in 1745 by Edmund Lee, eased this problem by automatically keeping the sails facing into the wind. It was simply a small rotor with many vanes mounted at right angles to the main rotor. If the mill was out of the wind direction, the fantail spun and forced the mill back into the wind.

The English in the late 1700's and early 1800's pioneered many improvements to the smock mills, which by that time were replacing the post mills in new construction. Metal was substituted for wood parts, and ball and roller bearings were introduced. The towers became larger and more complex. The forerunners of flyweight governors, used in "roller reefing sails" and

"patent sails", adjusted the sails in order to regulate the rotational speed of the rotor. It was a governor like one of those that become famous on James Watt's steam engine. The advent of these engines, however, spelled doom for the windmills, as the newer machines could perform any windmill's task more economically and reliably.

The use of windmills in North America began as colonists from Europe settled in the New World. Thus, the first mills were of the smock type and were found along the coastal regions in the Colonies and in Central America. After the American Civil War, people moved in great numbers out West across North America to settle the Great American Desert. This arid region provided countless acres of wide open land for anyone to tame if one natural obstacle could be overcome—lack of water. This led to the next great change in windmill design.

Figure 2.4 gives a general idea of what the classic Midwestern windmills looked like. Consisting of many vanes on a small rotor mounted atop a slender box frame, these mills lacked elegance compared to their elder counterparts. However, their purpose was not to grind grain but to pump water, and they did so quite well. So well, in fact, that the Great American Desert became the American Great Plains. By 1889, 77 windmill factories abounded in the United

States, and by 1903 windmill exports had become significant as other countries began to prefer the simple American designs [2].

As in Europe, however, the growth of industrialization marked the end of widespread use of wind power in the United States. In the years preceeding the Great Depression the electric motor slowly began to replace the windmill as the driving source for the pumps. Then the Rural Electrification Act (REA) of the 1930's provided main utility power to the small farm homesteads in a very short amount of time. Few of the remaining windmill manufacturers survived.

The end of widespread use of windmills to perform work directly did not mean the end of all wind machines. Wind turbines, used to drive electrical generators, became the focus of wind machine efforts. Efforts to analyze and improve the performance, power, and life of these turbines started in the early 1900's and continue today. A very large (1.25 MW) two-bladed HAWT was erected in Vermont during World War II and supplied power to the local commercial power grid for several months before a blade failure resulted in cancellation of the project [5]. Even though this Smith-Putnam project failed in the final analysis, it proved that wind turbines could be used to

produce commercially viable power.

More recent projects include the MOD series by the United States, with HAWT's ranging in size from the 100-kW MOD-0 in 1974 to the 3.2 MW MOD-5B by 1987. This last turbine is still supplying power to the Hawiian power grid [1]. Major projects are underway in Europe to utilize wind power for commercial consumption. The Netherlands, for example, should reach 150 MW of wind energy capacity by the end of 1991 and intend to have 1000 MW by 2000.

TECHNICAL REVIEW: The turbine used for this project has been studied in past years for its aerodynamic performance and power generating efficiency. Schetz et al. [6] describe using the turbine as the power source for a 1000-bushel apple cooling and storage system in 1978-79 at the VPI&SU Horticulture Farm. Although the system designed and tested for this process operated quite well, economics showed that use of wind power could not be justified for the relatively small amount of apples cooled and stored. Systems designed for larger capacities were found to be more practical.

Benim [7] performed the first thorough study of the turbine's aerodynamic performance while it was being used for the apple cooling project. He determined that the power coefficient, defined as

$$C_p = \frac{\text{Power}}{1/2\ \rho\ A\ V^3},$$

was dependent on the ratio of rotor tip speed to wind speed and reached a maximum value of 0.23 when this ratio was 6.5.

Hinerman [8] investigated the off-axis performance of the turbine. By measuring performance parameters at various yaw angles with respect to the wind direction, he determined that the power coefficient remained constant at all yaw angles for a given tip speed ratio.

Figard [4] performed wind tunnel tests on a 1/5 scale model of the wind turbine. He suggested that models such as that cannot give accurate predictions of full scale turbine performance, arriving at accuracies only within 10 to 15%. He also pointed out that use of the Navier-Stokes equations will accurately predict wake development. This can be useful in the study of windfarms, in which turbine wakes can dramatically affect the performance of nearby turbines.

Moses and Hawkins [9] performed a study in conjunction with Virginia Power in 1986-87 to determine the effects of the environment on the wind turbine over the course of one year. Although some problems were encountered, it was determined that the site was adequate for properly designed

wind turbines. Blade root stress versus wind speed data were taken, and it was found that a large fluctuating stress with a frequency of one per revolution occurred due to gravity and wind shear effects. The work for this thesis is based upon this study and further quantifies these findings.

The remainder of this technical review presents a cross section of research efforts in the wind turbine industry. Though many more studies have been and are now being performed in the following and other areas, a few have been included here to give an overview of what types of work is being done.

A large research effort is underway in the United States in the interest of providing data on blade, rotor, and tower loads and improving blade life. As part of the Cooperative Field Test Program for Wind Systems, Snow et al. [10] of Westinghouse Electric Corporation in cooperation with the Solar Energy Research Instiute (SERI) and the U.S. Department of Energy (DOE) operated a 600-kW wind turbine in Hawaii in 1987-88. Thorough investigations of blade stress and power output were performed, including a rainflow fatigue stress analysis. Also measured for future reference were the bedplate and tower loads.

Osgood and Coleman [11] report that HAWT's utilizing

free-teetered rotors experience blade bending moments an order-of-magnitude lower than fixed-teetered designs. Also, the yaw drive loads were found to be two orders-of-magnitude lower for a free-teetered system.

Efforts to develop computer models to predict blade loads have resulted in accurate codes. Earlier codes had trouble dealing with the stochastic, or turbulent, nature of practically all wind turbine inflow. The FLAP (Force and Loads Analysis Program) code is a widely known program that is under constant upgrading to provide more realistic simulations of blade dynamics. Wright, et al. [12, 13] describe the progress of model development from 1988-1989. It is clear that each passing year yields a more accurate and complete model. Follow up work includes expanding the model to include teetered rotors.

Other codes involving wind turbine rotors and towers include TEETER (accounts for teetered rotors), and YAWDYN (analyzes and predicts yaw loads and motion of the turbine). The latter was developed by Hansen and Cui, who describe the evolution of the software and examples of its use [14, 15, 16]. It should be pointed out that all of the above codes are in a continuous state of development, with refinements and expansions being researched. The state-of-the-art, then, will probably be different shortly after

this thesis is written.

Research into blade loads and life is not limited only to prediction and analysis of existing wind turbines. Efforts are underway to obtain optimal materials from which to construct blades with a longer fatigue life. Fatigue testing of various composites was jointly performed by Mohamadian, Graham, and Wang [17, 18, 19]. They determined that combination unidirectional and chopped mat polyvinylester composite laminates are good candidates for wind turbine blade applications. Also studied were vinylester laminates, and it was found that no significant differences exist in the fatigue life of these materials. Stiffness reduction in the materials was found closely related to different modes of damage under static and cyclic loadings.

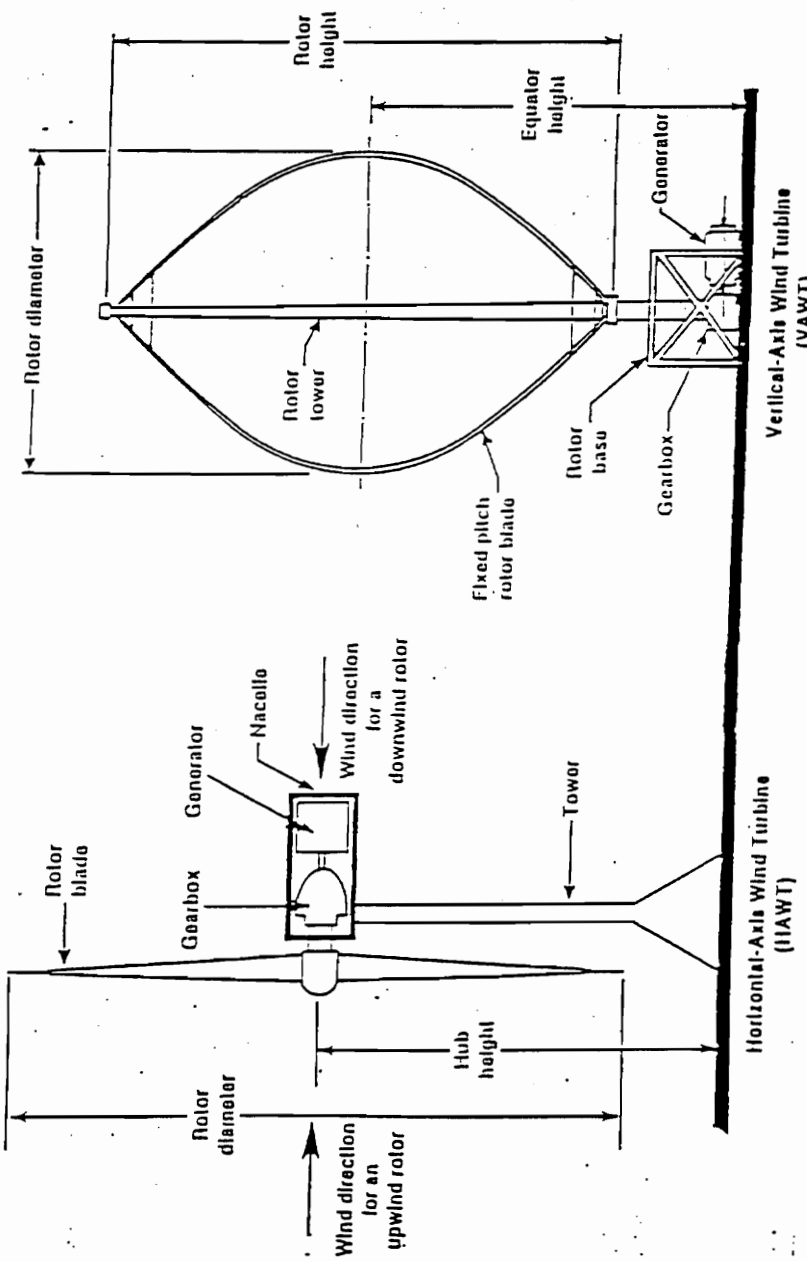

Figure 2.1 — Types of Wind Turbines
(Taken from reference 1)

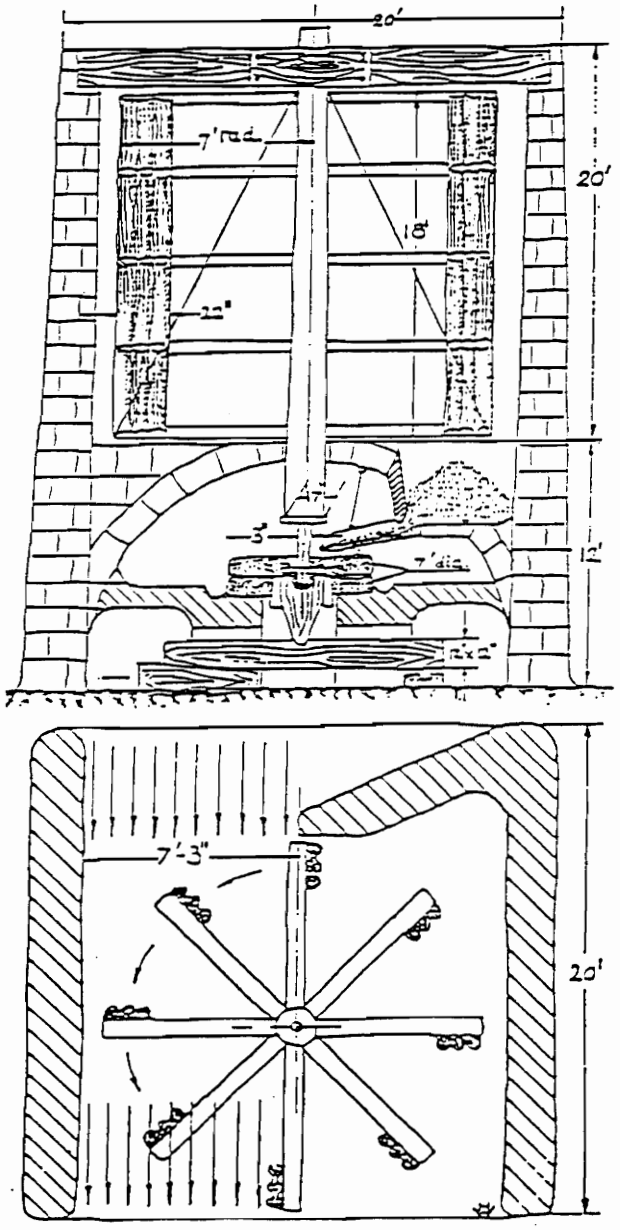

Figure 2.2 — Example of Persian Vertical Axis Windmill (Taken from reference 2)

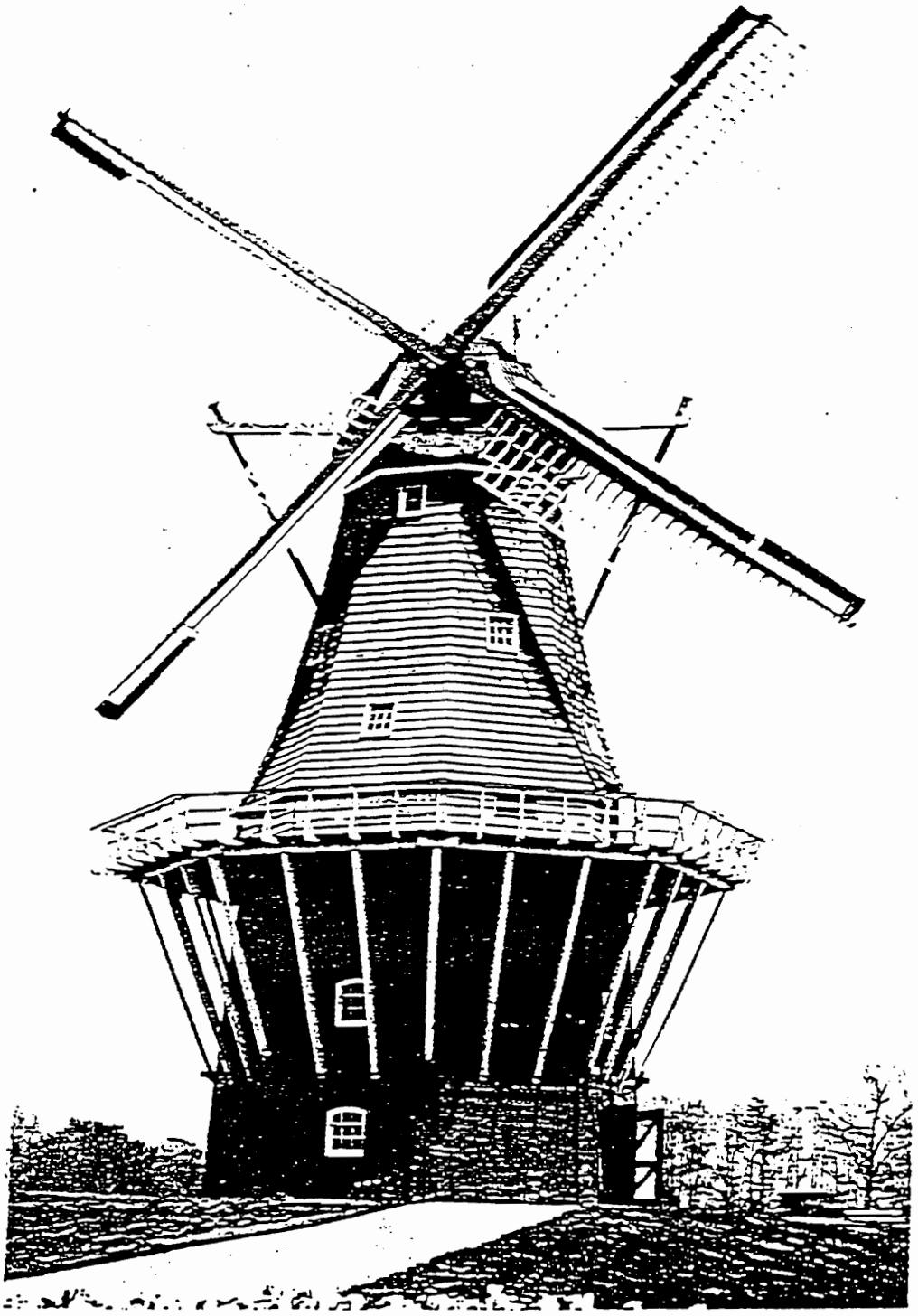

Figure 2.3 — Typical European Smock Mill
(Taken from reference 2)

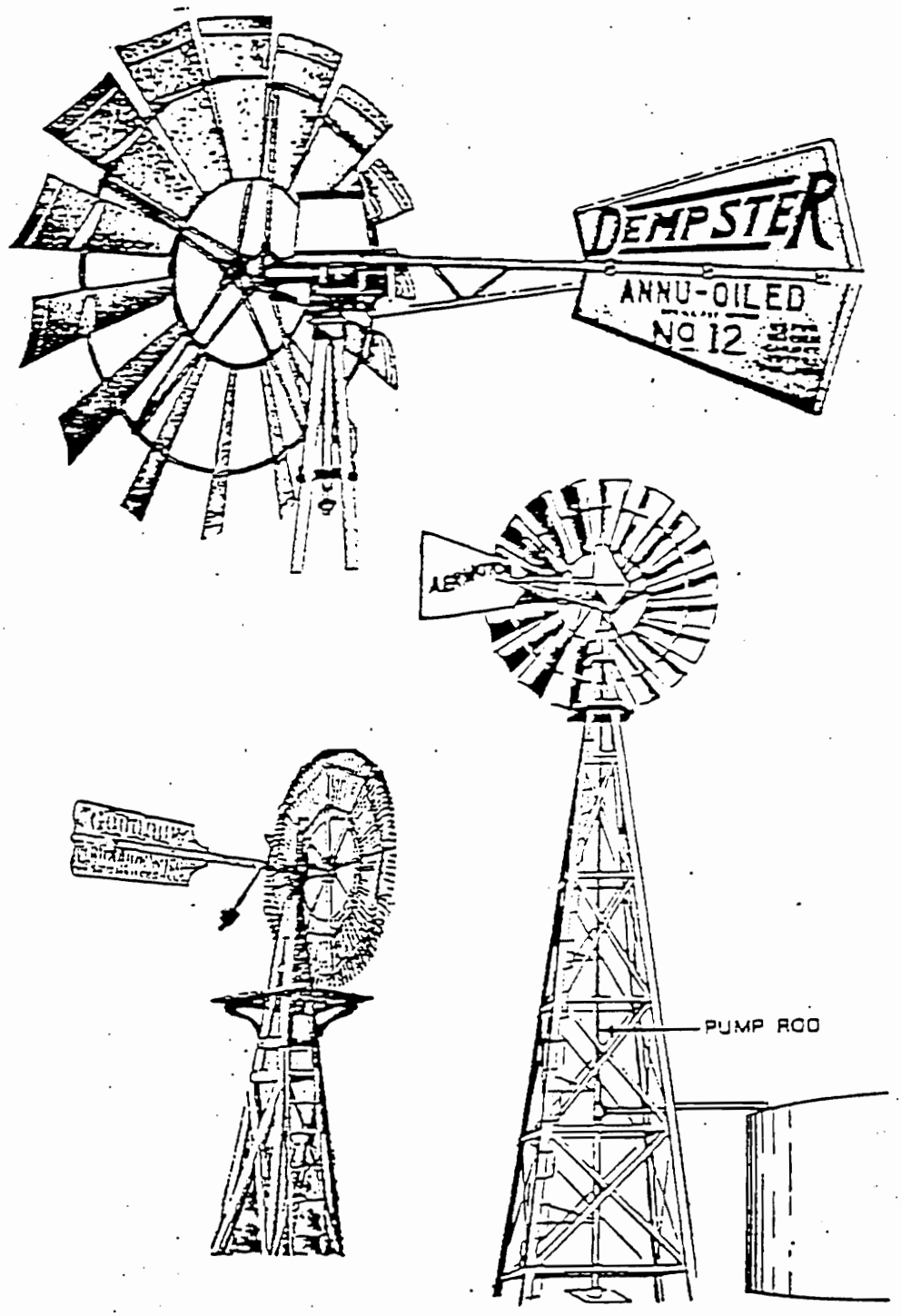

Figure 2.4 — Typical American Water Pumping Windmills
(Taken from reference 4)

CHAPTER 3 – EXPERIMENTAL APPARATUS

GENERAL DESCRIPTION: The major components of the wind turbine set-up are as follows:

- Wind turbine and generator
- Wind turbine control system
- Rotor instrumentation system
- Wind measuring system
- Data acquisition system

This chapter first describes the site on which the systems were placed for this project, followed by descriptions of each of the systems.

WIND TURBINE SITE: Figure 3.1 shows the site for the wind turbine. The tower, control building, and wind measuring support pole was placed several hundred feet up a hill from the nearest buildings in order to provide an uninterupted wind field. A standard electrical power line runs from the barn to the control building to provide power to operate the turbine's control and instrumentation systems as well as the data acquisition system.

The triangular cross section tower upon which the wind turbine sits is bolted to a 0.75-in. (1.91 cm) steel plate, which in turn is bolted to a concrete foundation. A grounding spike wired to both the tower and control system common terminal provides protection from lightning strikes.

Three guy wires attached slightly over halfway up the tower provide stability in the face of high winds. The tower is 20 ft (6.10 m) high and 14 ft (4.27 m) away from the control building. The control building is of simple frame and plywood construction and houses the turbine control panel and generator load, strain indicators and amplifiers for the wind measuring system, data acquisition system, and power receptacles. The pole upon which the original wind measuring assemblies are mounted is set 38 ft (11.6 m) away from the tower to provide adequate distance from the turbine blades to prevent erroneously measured wind speeds due to rotor interference. Although not shown in the photographs, the anemometer actually used to collect the wind speed data is mounted atop the control building. All wires are buried in 6-in. (15 cm) deep trenches for protection from weathering and interference from animals. The only exceptions to this are the leads from the original wind measuring system; however, these leads are kept at least 6 ft (1.8 m) above the ground.

WIND TURBINE AND GENERATOR: The wind turbine being studied in this project is an Elektro Model WVG 120G, built by the Elektro Company of Switzerland. It is an upwind, horizontal-axis turbine with a rated generator output of

10 kW at a wind speed of 30 mph (48.3 km/h). Blades were used that gave a blade tip diameter of 19.3 feet (5.89 m). That is, the three blades sweep out a circle of that diameter while rotating. The original blades were not used due to problems encountered in previous work. Appendix A gives the original specifications for the turbine and generator, while Figure 3.2 shows the blade cross sections at various positions along the blade. The machine is kept facing into the wind by a tail section. This tail section pivots 90° with respect to the turbine's main axis to turn the turbine out of the wind. This function can be operated both automatically and manually.

TURBINE CONTROL SYSTEM: The primary purpose of the control system is to automatically perform the pivoting of the tail and thus the turning of the turbine into and out of the wind. The control system for the wind turbine, also provided by the Elektro Company, consists of three major elements: the control panel, the control box, and the motor box. The control panel is located within the control building, while the two boxes are mounted on the tower itself. Start and stop buttons are provided on the control panel for manual control of the turbine, while the control box provides the automatic control of turbine

operation. The motor box houses the control motor and pulley arrangement.

Figure 3.3 presents the schematic wiring diagram for the control system, and Table 3.1 defines the symbols used. The turbine generator is located at the upper left, the control and motor boxes to the right of that, and the control panel to the lower right. The control motor box is not shown, but the motor itself is found at the upper right within the bounds of the control box.

Power for the control system is normally taken from the power line extended from the barn. A power strip provides on-site power cutout, while a switch box located in the barn allows the power to be cut from there. A small box, labelled "Control System Power", rectifies the alternating line current into direct current suitable for use by the control system. This box also houses a relay that automatically switches power for the control system from the main line to the generator output. That way, the turbine can be shut down under its own power in the event that there is a main power line failure or outage. This box is located in the control building and wires into the control panel as shown in Figure 3.3.

In order for the control motor to stop the turbine,

the switch marked SAB I in the control box must be closed, which is accomplished either manually or automatically. Examination of Figure 3.3 reveals that line 3 is a power line, line 4 is the stop line, and line 8 is the start line. Line 3 is taken directly from the power source and provides power to the SAB I solenoid and, ultimately, the motor. Line 4 provides a grounding path for the SAB I solenoid. Once the solenoid is grounded, the switch will close and power will be provided to the motor. The solenoid is grounded either by pressing the Stop button on the control panel, achieving an over-windspeed condition, or achieving an over-voltage condition. There are two metal plates hung at right angles to each other halfway up the tower. These are wind pressure switches and are wired into the control box as shown. When the wind reaches about 45 mph (72.4 km/h), one of the switches will be pushed enough to complete a grounding path via line 4 for SAB I, thus automatically activating the motor. There is also a switch, SAB II located in the control box, that will activate SAB I when the generator ouput reaches 160 V.

Starting the turbine is accomplished by pressing the Start button on the control panel. This action energizes the switch marked SJB I in the control panel and sends

power directly to the motor. However, if there is an automatic turbine trip activated, such as the wind pressure or over-voltage switch, the Start button will have no effect.

ROTOR INSTRUMENTATION SYSTEM: The rotor instrumentation system performs two primary functions. First, it measures the amount of stress in the rotor blades through the use of strain gages mounted on two of the blades. Second, it provides a way of determining the angular position of the blades at any given time.

Resistance-type strain gages are used to detect the stresses in the wooden turbine blades, albeit indirectly. In order to facilitate gage installation and performance, 12-in. (30.5 cm) aluminum blade extenders are placed between the rotor hub and each blade. This provides a smooth, homogeneous material to which to bond the gages. Also, since the modulus of elasiticity for aluminum is consistent, unlike that for wood, accurate stresses, and therefore bending moments, may be calculated via the strain data since

$$\sigma = E\epsilon$$

and

$$M = \frac{\sigma I}{c},$$

where σ is the stress, E is the modulus of elasticity, ϵ is the strain, M is the bending moment, I is the moment of intertia of the extender's cross section, and c is the distance from the neutral bending plane to the point of maximum stress. Figure 3.4 shows a schematic of the apparatus required to obtain the blade stress information. Two of the three blades are equipped with strain gages. Each of those blades has two gages on each side of the blade extender. When combined in a full Wheatstone bridge arrangement, maximum sensitivity and temperature compensation for the gages is achieved. In other words, the change in bridge output voltage is maximized and the effects of ambient temperature change on the bridge output voltage are eliminated.

The signals from each bridge are sent to an on-rotor amplifier in order to boost the low-level bridge output voltage. The amplifier for blade 1, or Amp 1, provides a gain of 63.5, while the gain for Amp 2 is 33.2. These amplifiers were used for this purpose in past experiments with this turbine [9], and due to their age the gains have since decreased. However, the gains are still large enough to warrant keeping these amplifiers for this project. These amplifiers are mounted to the interior of a housing

which is fixed to the rotor hub and thus are part of the rotating system.

The corresponding stationary system consists of a slip ring and the wiring required to transmit the turbine instrumentation system signals to the data acquisition system. The slip ring, donated previously by Poly-Scientific Division of Litton Industries, is a 40-channel instrument roughly 0.5 in. (1.3 cm) in diameter and 1.5 in. (3.8 cm) long. Since many more channels are available than are needed, the signals crossing the slip ring use multiple channels each, which reduces the noise-to-signal ratio across the slip ring to a very low level. Combined with the on-rotor amplification of the blade bridge output, the effects of transmission noise are virtually eliminated and can be ignored for the purposes of this project.

From the stationary side of the slip ring, the signal wires travel through the main axis of the turbine and down through the vertical shaft around which the turbine pivots. Care had to be taken as the signal wires tended to wrap around the brake cable as the turbine turned with the wind. Periodic unwinding of the wires was necessary to avoid the breaking of those wires.

A small box, labelled "Rotor Instrumentation Box", provides both the power for the rotor instrumentation system and the screw terminals for connecting the leads from the instrumentation systems to the data acquisition system. Also housed within this box is a frequency-to-voltage converter used to convert the pulses from the angular position indicator to an analog voltage that can be converted to the rotational speed of the rotor. This feature had problems in the past and is not in use at present. Instead, the rotational speed is determined by measuring the time between pulses of the angular position indicator trace.

The strain gages on the two instrumented blades needed to be calibrated so that a given bridge output voltage could be converted to a corresponding bending moment on the blade. Each blade was calibrated in an identical manner. This calibration procedure involved bolting a blade to its aluminum blade extender and clamping the entire assembly in a cantilever fashion to a table. The leads from the strain gages were fashioned into a full Wheatstone bridge, and this bridge was then wired to the power supply and specified on-rotor amplifier. The amplifier was in turn wired to a digital voltmeter (DVM). An aluminum cube with

a mass of 6.50 lbm (2.95 kg), was then placed at known distances from the strain gages. This provided a known bending moment, which produced a characteristic output voltage measured by the DVM. The calibration was repeated for each blade, but comparisions to the first set of tests yielded no significant variations in the results. Table 3.2 lists the data gathered for each of the instrumented blades during this procedure. Figures 3.5 and 3.6 display this information in graphical form along with the linear regression lines of the data. The correlations are quite good, being 0.9998 and 0.9999 for blades 1 and 2, respectively, indicating a very good linear curve-fit. Difficulties were encountered with the signals from blade 2 during on-site data acquisition and little reliability could be assessed to them. Therefore, no attempt is made at present to include these data.

The angular position of the rotor blade is an important piece of information to have since stress in a given blade will vary as the blade travels through one revolution due to gravity and wind shear effects. This information is found with the help of light emitting and detecting diodes, collectively termed the blade position indicator (BPI). As shown in Figure 3.7, these diodes face

each other from opposite arms of a U-shaped plastic chip, which is fixed to the stationary wiring tube extending through the rotor hub. For clarity, the bracket supporting the chip is not shown. A metal obstruction is fastened to the rotor hub itself such that as the rotor turns, the obstruction passes between the arms of the chip. This interferes with the light beam passing from one diode to the other, and this interference is detected by a change in voltage output of the detector diode. The change in this voltage is found when blade 1 is between the 7:30 and 9:00 o'clock positions. Keeping in mind that blade 2 is that blade just clockwise from blade 1, its position can also be determined at any given moment if necessary through examination of the BPI trace. In other words, when the BPI trips and its trace indicates an obstruction, blade 2 is between the 11:30 and 1:00 o'clock positions. The normal voltages for the BPI trace are roughly 6 V in the non-tripped state and roughly 13 V in the tripped state. A potentiometer is employed to reduce these values to within the analog input range of the data acquisition system.

WIND MEASURING SYSTEM: The purpose of the wind measuring system (WMS) is to determine the speed of the wind field at the turbine site. This was originally done at the two

elevations corresponding to the mean blade radius in order to account for variations in wind speed due to altitude, or wind shear. Since one objective of this project was to assess the impact of rapidly fluctuating wind velocities on the wind turbine rotor blades, the dynamic response of the WMS devices must be such that the devices are able to detect such changes accurately.

The original wind measuring system is based on a drag sphere concept. The drag sphere, in this case a plastic toilet tank float, is mounted atop a small aluminum column having a square cross section. This sphere/column combination is termed a WMS assembly. The column is fitted with four strain gages, one on each side, near the base. Two gages on each side would have provided more sensitivity, but due to space considerations only one gage per side is feasible. The gages on opposite sides of the column are configured in a half-bridge arrangement, giving maximum sensitivity and temperature compensation. Thus, two bridges are required for each assembly and four are required in all. The force of the wind on the whole assembly will bend the column, causing the gages to detect the resulting stress in the plane they measure since each bridge can detect bending in one plane only. By

calibrating each bridge on both assemblies in a wind tunnel, an accurate assessment of wind speed in each plane may be made in the field. Vectorial addition of the wind speeds found by the two bridges on a given assembly results in the actual wind speed and direction. Two assemblies are used in order to account for variations in wind velocity due to altitude, or wind shear. They are mounted to a support bracket, which in turn is mounted to a wooden telephone-type pole. The two assemblies are arranged vertically such that they are at heights corresponding to the mean radius of the rotor blade circle. The leads from the strain gages are run to Measurements Group P-3500 strain indicators. These devices provide the half-bridge configuration required. They also provide a 2-V bridge excitation voltage and display the strain detected by the gages as well as output a voltage signal proportional to the measured strain. These signals are then amplified before being sent to the data acquisition system so as to achieve better resolution of the acquired data.

The design process of the aluminum columns used in the WMS assemblies partly centered around ending up with as high a natural frequency as possible. Assemblies with a high natural frequency will not tend to resonate in a

rapidly fluctuating wind condition. The assembly is driven at the frequency of the fluctuating wind speed, thus if the natural frequency of the assembly equals this "wind frequency" the assembly will resonate. Thus, the recorded strains will be due to both the drag of the assembly in the wind field and the increased vibration amplitude caused by the resonant condition. The natural frequency of the assembly should then be made as high as possible so as to be higher than any likely wind frequency.

Unfortunately, high natural frequencies imply high stiffness, which results in low sensitivities [20]. In other words, the stiffer the column becomes, the less it will bend in a given wind speed. Thus the detected strains will be smaller, and the deflection bridge output will be smaller for a given wind speed. This fact is utilized in strain gage selection and determining an order-of-magnitude estimate of device geometry. Also of importance to consider is the damping ratio of the device. As this ratio increases, the effective (damped) natural frequency decreases as

$$\omega_d = \omega_n\sqrt{1 - \zeta^2} \quad ,$$

where ω_d is the damped natural frequency, ω_n is the undamped

natural frequency, and ζ is the damping ratio. For small ζ, the effective natural frequency is approximated by the undamped natural frequency.

The WMS assembly is bolted at the base of the aluminum column to the support structure. Thus, for modeling purposes, it can be treated as a clamped-free beam system. That is, one end is clamped while the other end is free to vibrate. The equation governing the natural frequency of beams is given by

$$\omega_n = (\beta_n l)^2 \sqrt{\frac{EI}{ml^4}} \quad ,$$

where E is the modulus of elasticity, I is the moment of inertia, m is the mass per unit length of the beam, and l is the length of the beam. The quantity $(\beta_n l)$ characterizes the end conditions of the beam in question, be they clamped, free, or pinned. In the case of a clamped-free beam system as found here, this expression retains a value of 1.8751 [21]. This model of the natural frequency of the WMS assembly does not take into account the extra mass present in the drag sphere but was used to obtain rough estimates of acceptable column geometry. A computer model was generated to explore the effects of length and width on the natural frequency based on the above equation. It was

found that the natural frequency increases with width and decreases with length, and a 0.5 in. (1.27 cm) square cross section best met the high natural frequency requirement without becoming too cumbersome. Lengths from 5 in. (12.7 cm) to 15 in. (38.1 cm) were used, with resulting frequencies ranging from 1949 Hz to 1125 Hz.

As noted above, the shorter the column the higher the natural frequency. However, the bending moment at the base of the column will decrease as the column becomes shorter. This results in lower strain at the column base, and since such strain is quite small for this magnitude of bending, the use of short columns is not advantageous. Thus, a tradeoff is seen between higher natural frequency and higher strain. In other words, the sensitivity of the device decreases as the natural frequency increases. Another computer model was created to test the effects of column length and wind speed on strain at the base of the column. Column lengths identical to those above were used, as were wind speeds ranging from 10 ft/s (3.05 m/s) to 100 ft/s (30.5 m/s). These wind speeds cover the range in which the turbine will operate safely. The bending force was assumed to come only from the drag on the float itself; no drag on the column was considered. The results, then,

will be conservative and the strains smaller than calculated. The float was approximated as a sphere, and in the range of interest the flow was found to be laminar. Thus, the drag coefficient was taken to equal 0.47 [22]. The drag forces were calculated to range from 0.00551 lbf (0.0247 N) to 0.551 lbf (2.47 N). These forces were then used to find the corresponding bending moments, bending stresses, and finally the bending strains. As expected, the shorter columns resulted in lower strains than the longer columns. A column of length 12 in. (30.5 cm) was chosen for its ability to produce adequate strains (0.366 $\mu\epsilon$ to 36.5 $\mu\epsilon$) and its high natural frequency (1258 Hz).

The selection of appropriate strain gages for the WMS assemblies mainly involved obtaining gages of adequate size. Since the assemblies were designed to be 0.5 in. (1.3 cm) wide on each side, the gages had to be less wide than this value. Micro-Measurements Division Model EA-13-250AE-350 Option E gages were selected due to their size and general purpose nature. They also contain large solder tabs for ease of integration with the lead wires. Once mounted on the assemblies lead wires were soldered in place and the gages were covered with a

waterproof rubber coating for protection from the weather when installed on site.

All of the preceeding analyses for the WMS assemblies were used to produce the two devices required. However, experimental data were needed to determine the actual natural frequency and sensitvity. The natural frequency response was obtained by clamping the base of an assembly and wiring the gages in the amplified half-bridge configuration described above. The output from the amplifiers was fed to a strip chart recorder and the free vibration response recorded. Figure 3.8 shows a representative trace acquired using a chart speed of 3.94 in./s (10 cm/s). The distance between successive peaks is seen to be roughly 0.1 in. (0.25 cm), giving an average natural period of roughly 0.025 s, which translates to a natural frequency of about 40 Hz. It should be noted that this value is only 3.2% of that predicted through the preceeding analysis. This is due to the fact that the additional mass of the drag sphere on the end of the column was unaccounted for previously and slowed the response of the assembly considerably. This natural frequency was judged acceptable nonetheless since analysis of previously gathered wind speed data [9] revealed wind frequencies

averaging no more than 20 Hz. Thus, there will be at least a 2:1 margin of safety against resonance of the WMS assemblies. Nevertheless, a model of a mass atop a massless column would have predicted the behavior more accurately.

Using logrithmic decrement techniques [21], the damping ratio is found to be 0.008. This indicates that the effective natural frequcency will be 0.9996 as large as the undamped natural frequency and that any effect of damping on the natural frequency response of the device is negligible.

Determination of the strain gage response entailed finding the relationships between the voltage output of each strain gage bridge and wind speed. In order to assure consistency between experimental testing and field work and to get the most accurate results possible, each pair of gages was assigned its own P-3500 strain indicator and amplifier. Each pair of gages was calibrated separately in a subsonic wind tunnel to find their characteristic voltage/wind speed relationship. The calibration procedure first involved clamping a given assembly inside the wind tunnel such that the gage pair to be calibrated was in-line with the air flow. Then the strain indicators and amplifiers were connected as they would be in the field,

with the exception of using a DVM in place of the data acquisition system. The wind tunnel uses a velocity pressure manometer to indicate wind speed information as a matter of simplicity. The wind speed, V, can be obtained through the following equation:

$$p_v = \frac{\rho V^2}{2}$$

The wind speed is thus a function of the air density at the time of measurement. Therefore, all calibration curves are in terms of velocity pressure, as the actual wind velocity in the field will most likely be different than that found in the tunnel for a given bridge output voltage. A given velocity pressure produces a given bridge voltage output. This condition allows the calibration curves obtained in the tunnel to be directly applicable to data taken in the field. Once the velocity pressure in the field is known, the pressure and temperature of the air at the time of data acquisition can be used to find the density of the air and thus the wind speed.

It was found that the output voltage did not stay constant at a given wind speed in the tunnel. This discrepancy was most likely due to the age of the tunnel. With the fan and its driving motor not in the newest of

conditions it is likely that, although the velocity pressure manometer could not register any changes, the motor speed fluctuated slightly even when the speed control dial was left alone. Multiple runs for each strain gage bridge were conducted, with average calibration curves generated.

Figures 3.9-3.12 show the calibration curves for each of the strain gage bridges, while Table 3.3 lists the coordinates of each data point. The curves labeled as "WMS 1" indicate the assembly mounted at the upper elevation, while the curves labeled as "WMS 2" indicate the assembly mounted at the lower elevation. The terms "Bolt Direction" and "Crosswise Direction" indicate the orientation of the gages with respect to the bolt holes by which the assemblies are mounted to the support bracket. The "Bolt Direction" is that in which the bolt holes run, while the "Crosswise Direction" is that perpendicular to the "Bolt Direction". The correlations for each curve are in the range of 0.9946 to 0.9991, indicating very good curve fits.

The mounting bracket used to support the two WMS assemblies consists of two pieces of aluminum angle bar bolted to a 13 ft (3.96 m) aluminum box bar. This entire

assembly is fastened to the WMS pole with lag screws, as shown in Figure 3.13. In spite of the length of the leads running from the WMS assemblies on the pole to the strain indicators in the control building, no great voltage drop was expected. Each lead is 30-gauge copper wire, having a resistance of 169 Ω per 1000 ft (169 Ω per 305 m). With the WMS 1 leads about 75 ft (23 m) long, an additional resistance of only 12.7 Ω is added to the system. Since the strain gages themselves have a resistance of 350 Ω, the change in resistance is 3.62 %. The voltage drop, then, is 3.62 %, while for the WMS 2 leads which were 63 ft (19 m) long, the voltage drop becomes 3.04 %. The acquired voltages are adjusted upwards accordingly to determine the voltage at the gages.

Problems were encountered with this wind measuring system while running on-site. Significant quantities of electromagnetic noise from the main power line contaminated the WMS signal to such a degree that the signal was not discernible; consequently, all of the wind speed values were approximately the same no matter what the wind conditions actually were. Efforts to correct this problem yielded no appreciable reduction in the noise-to-signal ratio, so an alternate method was employed to obtain some

assessment of the wind speed at the site.

A Weathermeasure Model 2011 three-cup rotating anemometer provided wind speed data without any noticeable line noise effects. The calibration curve, determined previously by Wilks [23], is given in Figure 3.14. This was mounted atop the control building at a level slightly higher than that of the original lower WMS assembly. Though the inertia of the rotating anemometer made rapid wind speed fluctuations difficult to measure, much of the data taken involved fairly steady wind conditions.

DATA ACQUISITION SYSTEM: The data acquisition system (DAS) collects and stores the data required for this project. These data originally included the pulse train from the BPI, the two amplified rotor blade strain gage bridge outputs, and the four WMS strain gage bridge outputs, making a total of seven input channels. As shown in Figure 3.14, the data acquired after the alternate wind measuring system were employed are the same except the four WMS signal are replaced by the single anemometer signal for a total of four input channels. These channels are defined in

Table 3.4. An IBM PC located at the site and fitted with a

data acquisition board performs the collection and storage operations.

The DAS is built around a Data Translation DT2811-PGH multi-function I/O board installed in the PC. This board has two 12-bit digital-to-analog converters (DAC's) and a 12-bit analog-to-digital converter (ADC) capable of sampling rates as high as 27.5 kHz, though a sampling rate of only 100 Hz is used here. This ADC can handle up to sixteen single-ended or eight differential-input channels via jumper blocks on the board. Because the wind turbine is operated in an electrically exposed condition and no more than eight channels are needed, the channels are used in the differential-input mode to help eliminate noise during data acquisition. Sixteen digital I/O lines are available for connection to other machines, though this feature is not needed for this project. The board is programmable for gains of 1, 2, 4, or 8. This board employs the the successive approximation technique to perform the ADC operations and can be programmed in any language capable of accessing the PC's I/O registers, but BASIC is used here.

The software employed to run the DAS board is Data Translation's LPCLAB package. This provides many routines

that take care of the details of controlling the individual data registers. By simply calling a needed subroutine with appropriate parameters, the many instructions required to manipulate the registers and data are carried out. The complicated programming has already been done by Data Translation. All that is required is to know in advance what specifics the task requires, such as Direct Memory Access (DMA), Single or Block Operation, and triggering just to name a few options. The task for the DAS did not require the use of advanced acquisition functions, so many of the capabilities of the software were not employed. The program used is a modified version of that provided with the LPCLAB software package.

The ADC routines all return what is called an Analog Data Value (ADV). This is the digital representation of the analog signal sampled by the ADC. To get the actual analog voltage supplied to the ADC, the following equation is used [24]:

$$\text{Analog Voltage} = \text{ADV} \times \left[\frac{\text{PFS} - \text{MFS}}{\text{NOC}}\right] + \text{MFS}$$

The range of voltages is based on the board's amplifier gain and whether or not the voltages are uni- or bi-polar.

Since most of the signals can have either positive or negative values, bi-polar coding is used. Thus, PFS equals +2.5 and MFS equals -2.5. A gain of 1 is employed, giving an unamplified voltage range of ±2.50 V. The NOC value is based on the number of bits the ADC contains. Since the board uses a 12-bit converter, there are 4096 possible combinations, or steps, giving a resolution of 1.22 mV/step. That is, each time the measured voltage increases by 1.22 mV, the ADV increases by 1. A routine is employed in the program to automatically perform the conversion from the ADV's to the actual voltages in the data sets.

The program used to control the board not only acquires the seven data channels, but also stores the data on floppy diskette. The program collects the data beginning with Channel 0 and continues up through Channel 3. It then returns to Channel 0 and begins again. It cycles through the four channels in this way 1250 times for a total of 5000 data points per data set. This gives the desired sampling period of 10 s and an effective sampling rate per channel of 125 Hz. The period between successively-acquired data points is 2.0 ms. After the run is completed the array is written to a new data file.

Figure 3.1 — View of Wind Turbine Site

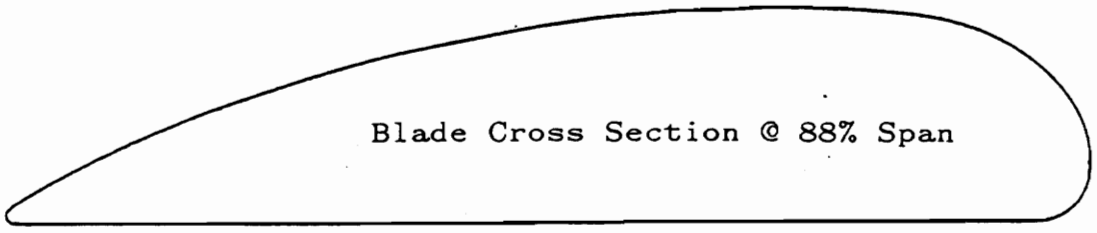

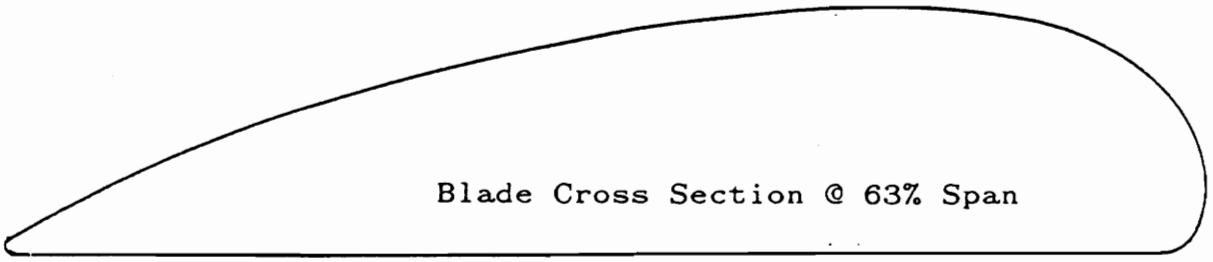

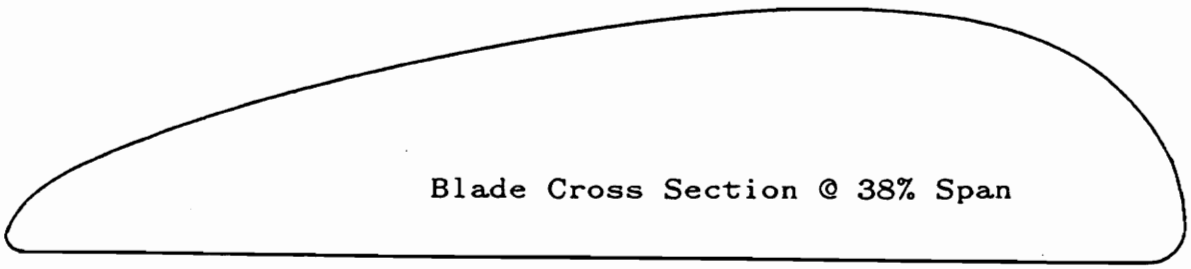

Figure 3.2 — Rotor Blade Cross Sections

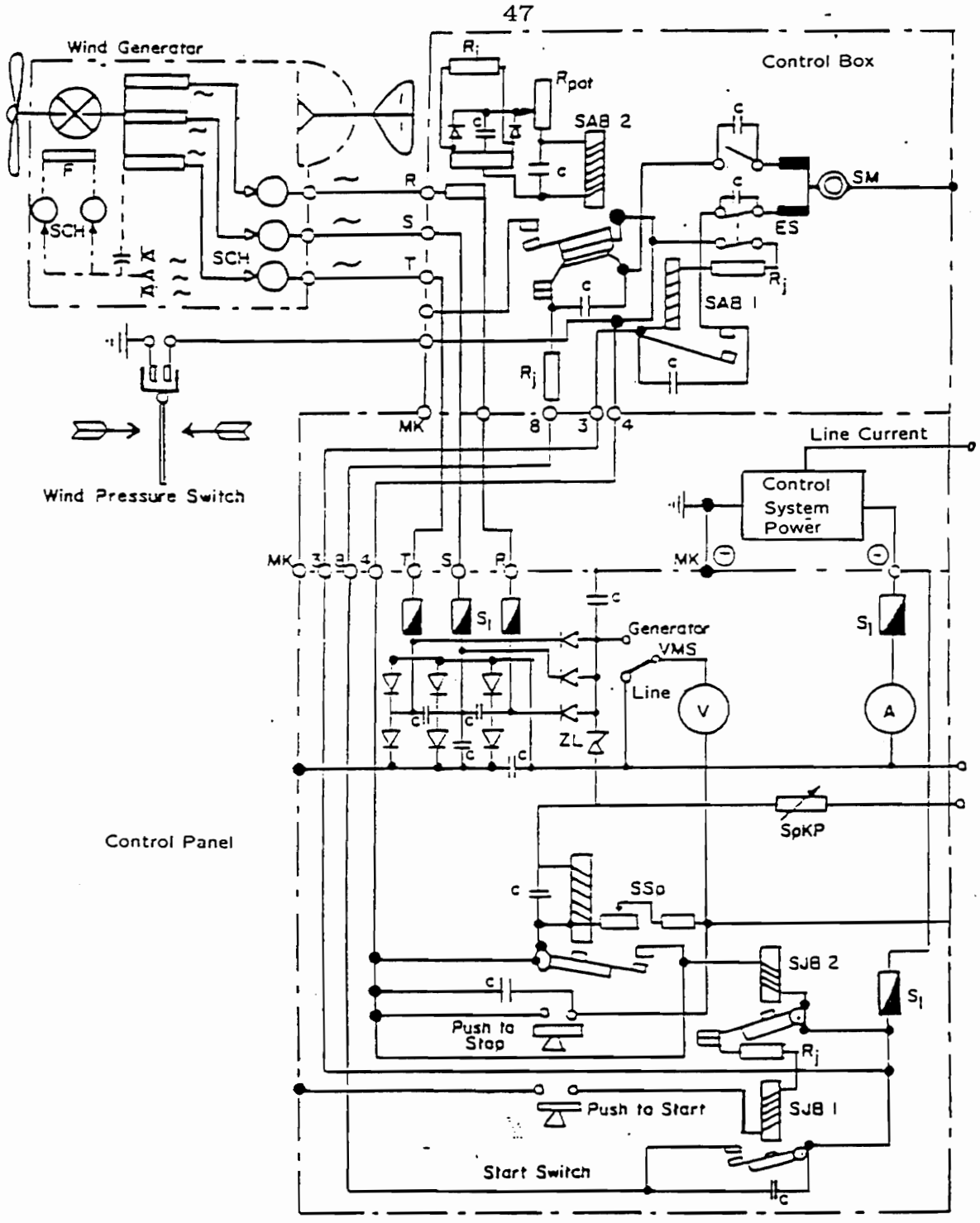

Figure 3.3 — Control System Wiring Schematic
(Adapted from reference 14)

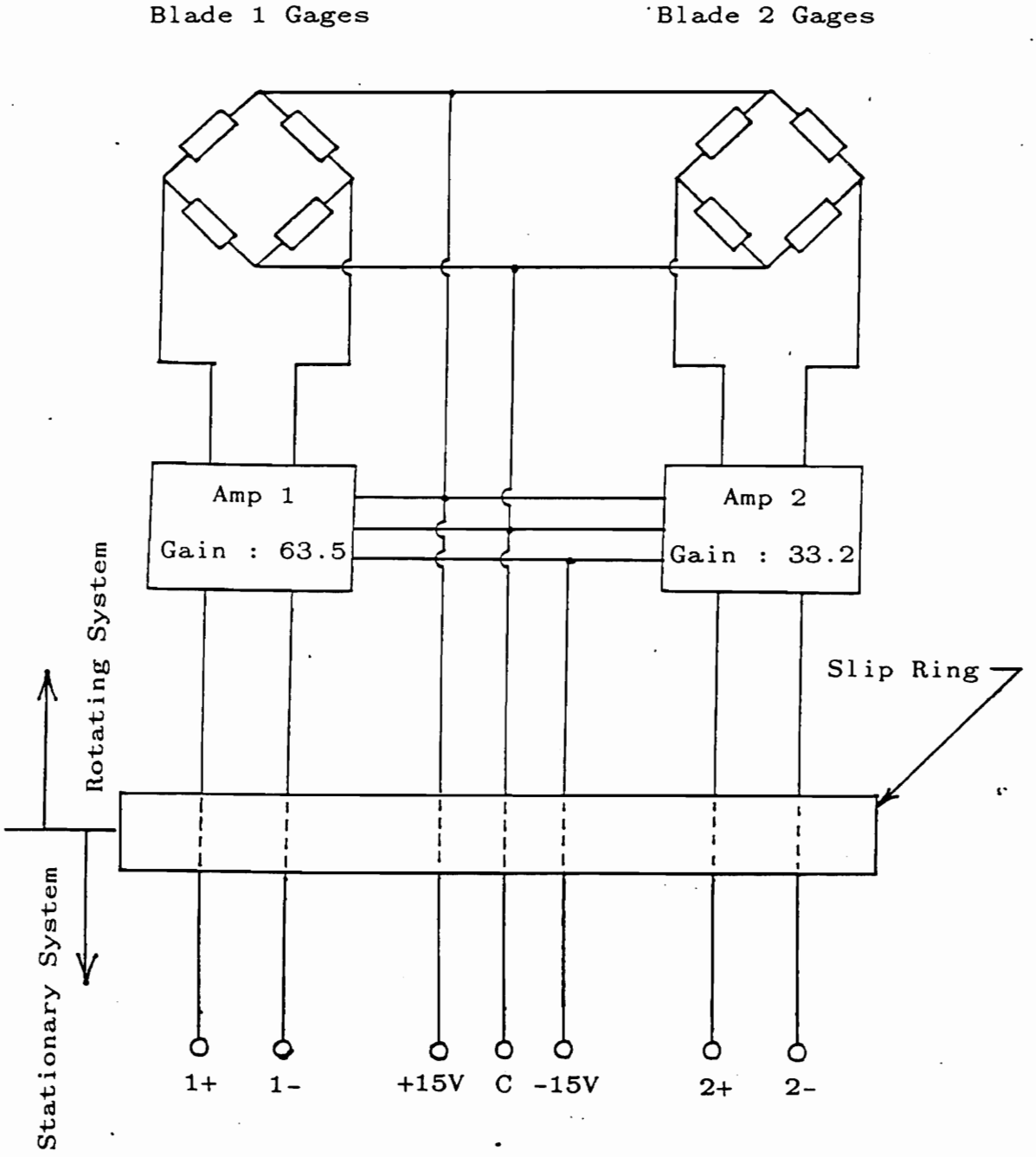

Figure 3.4 — Blade Instrumentation Schematic

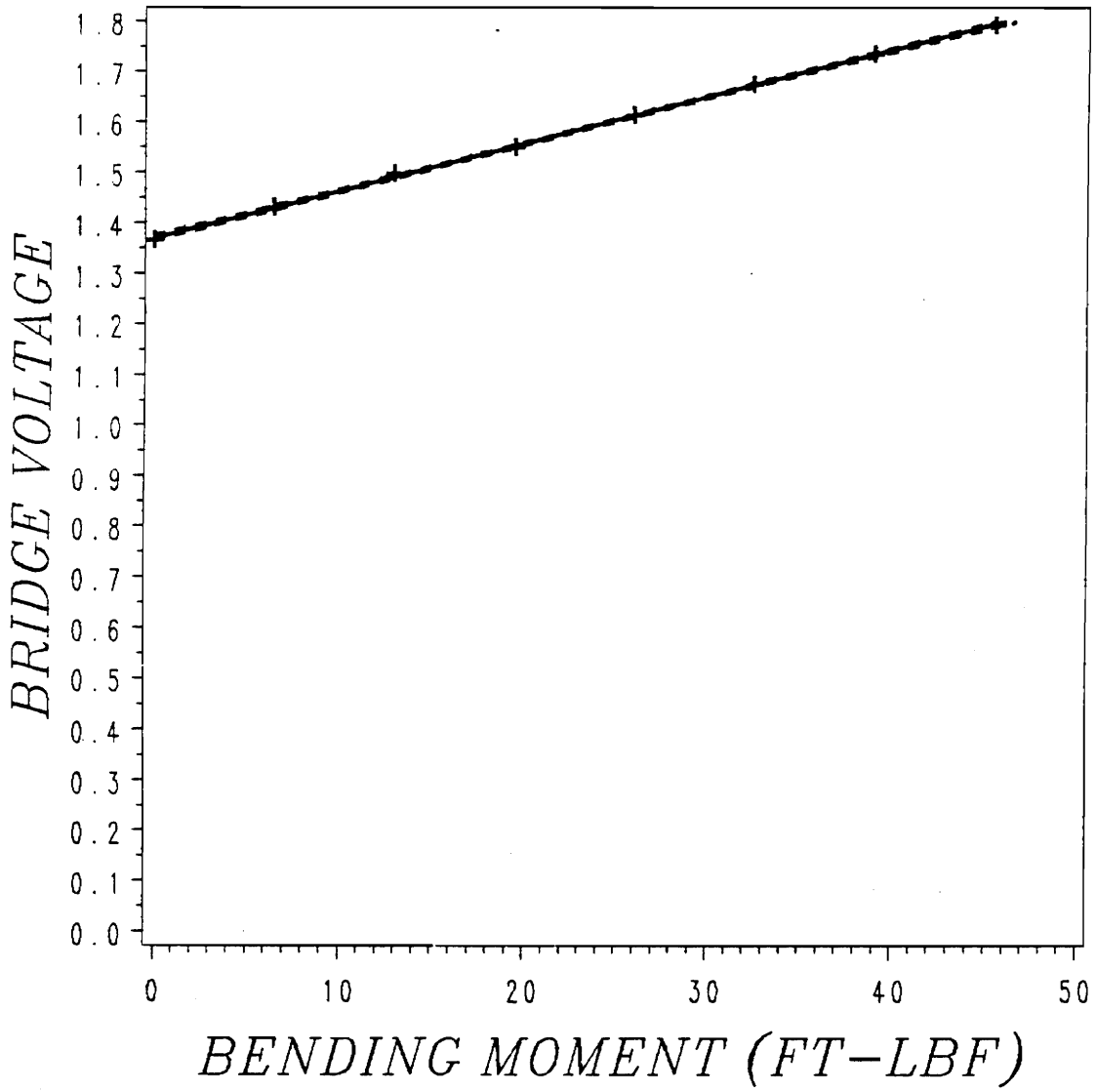

Figure 3.5 — Calibration Curve - Blade 1

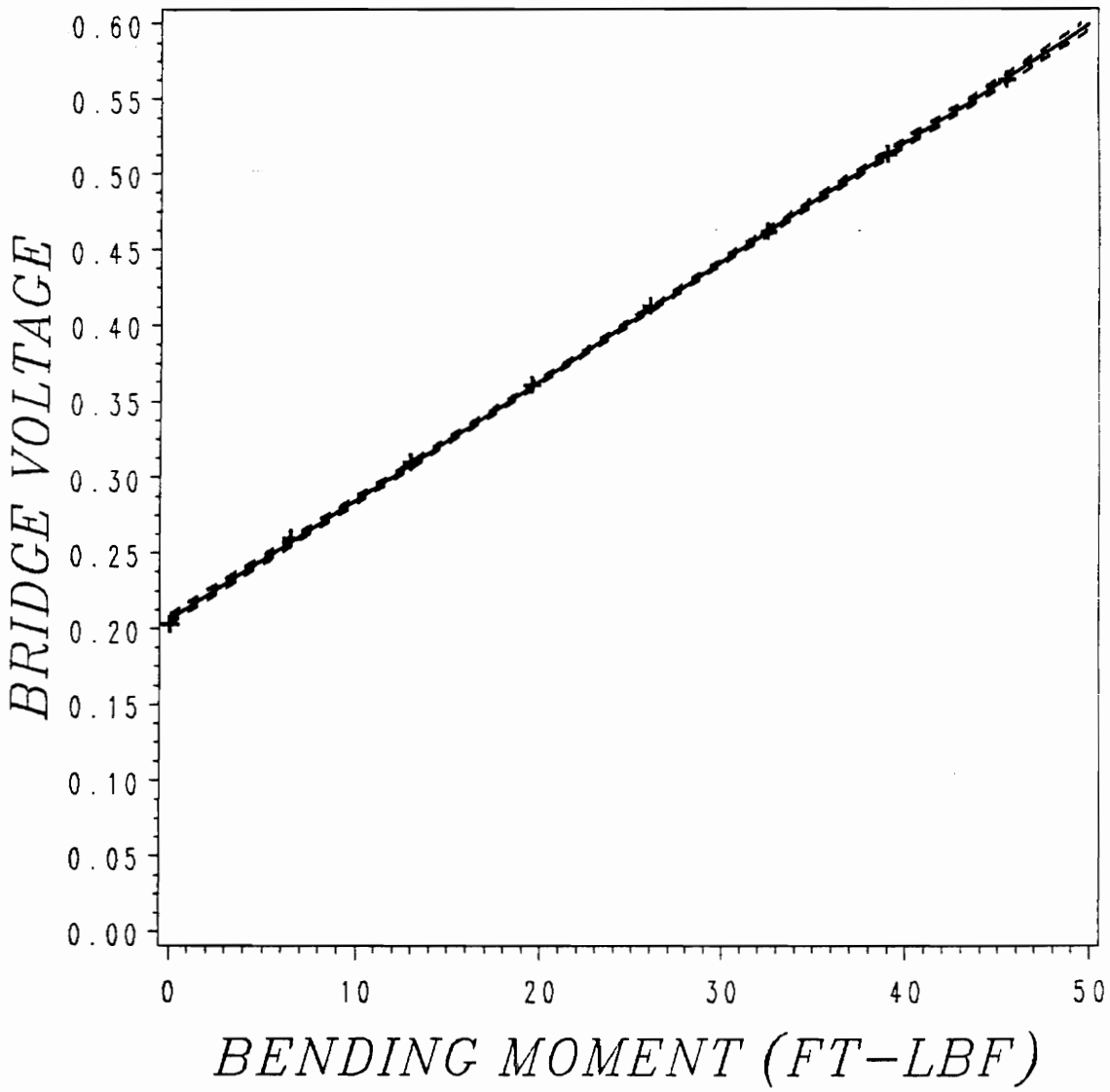

Figure 3.6 — Calibration Curve - Blade 2

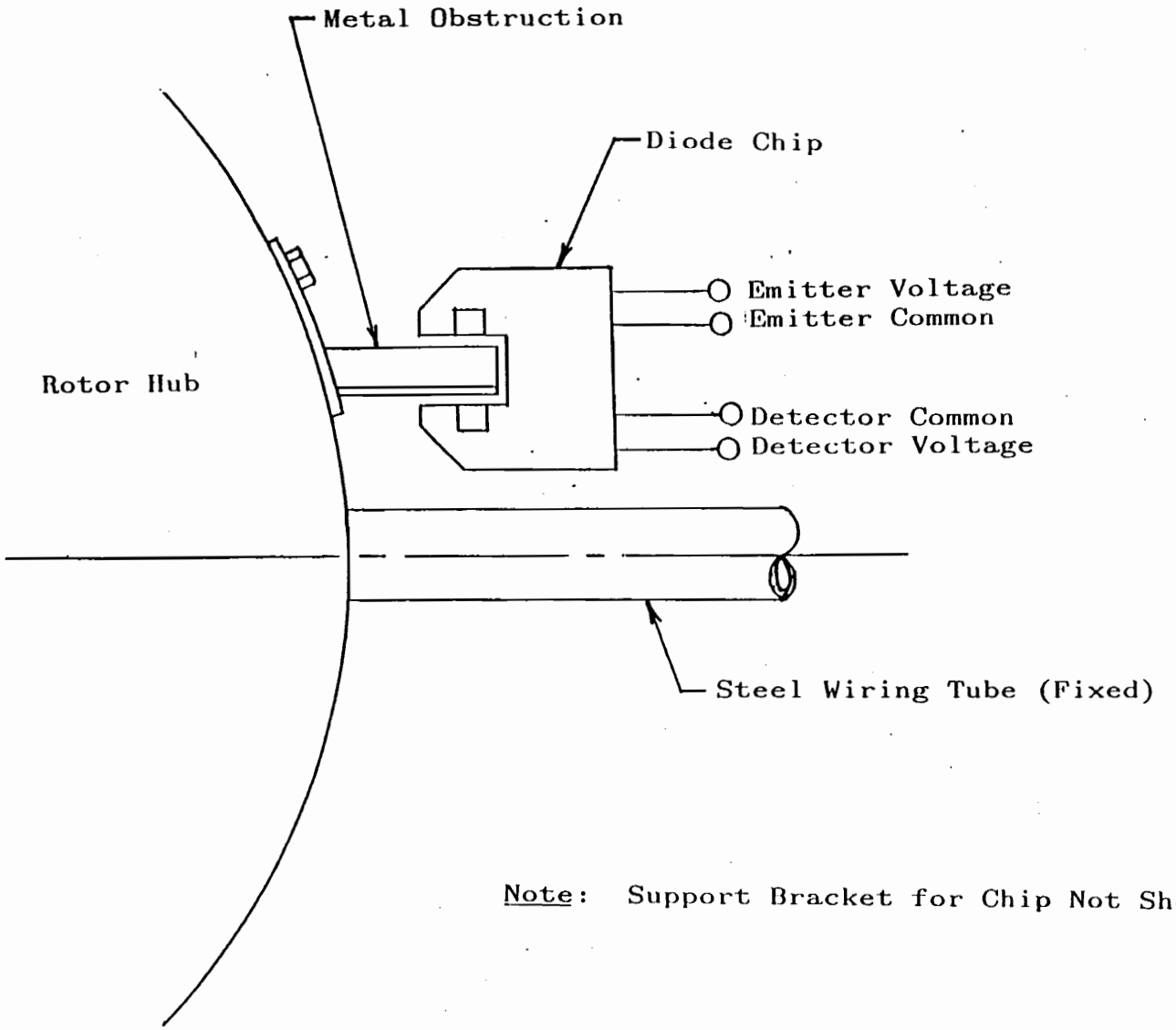

Note: Support Bracket for Chip Not Shown

Figure 3.7 — Blade Position Indicator Diagram

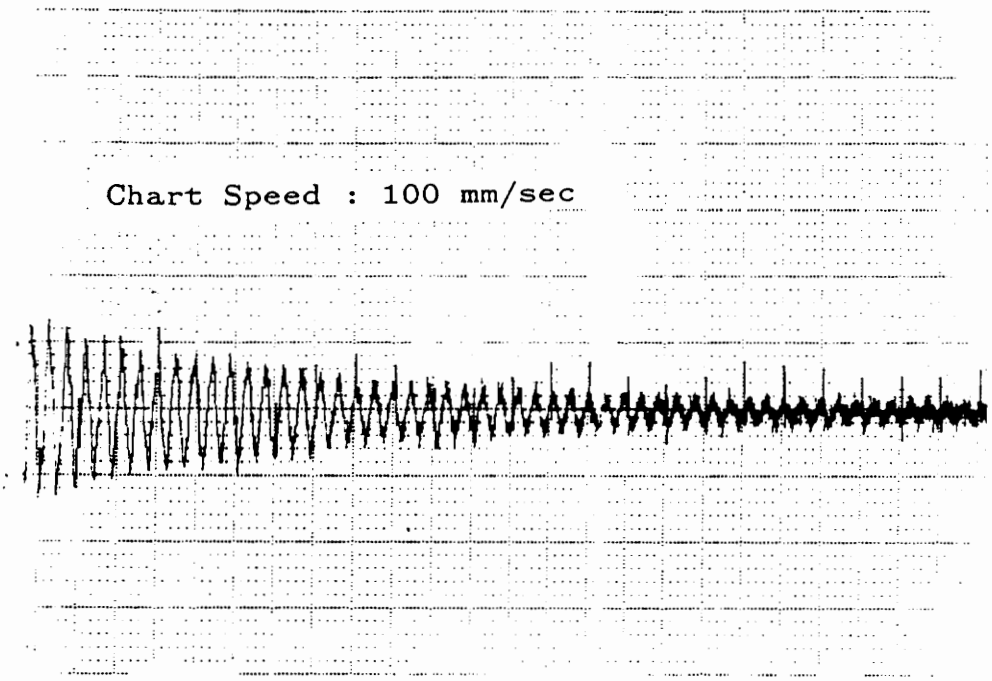

Figure 3.8 — Typical Free Response of WMS Assemblies

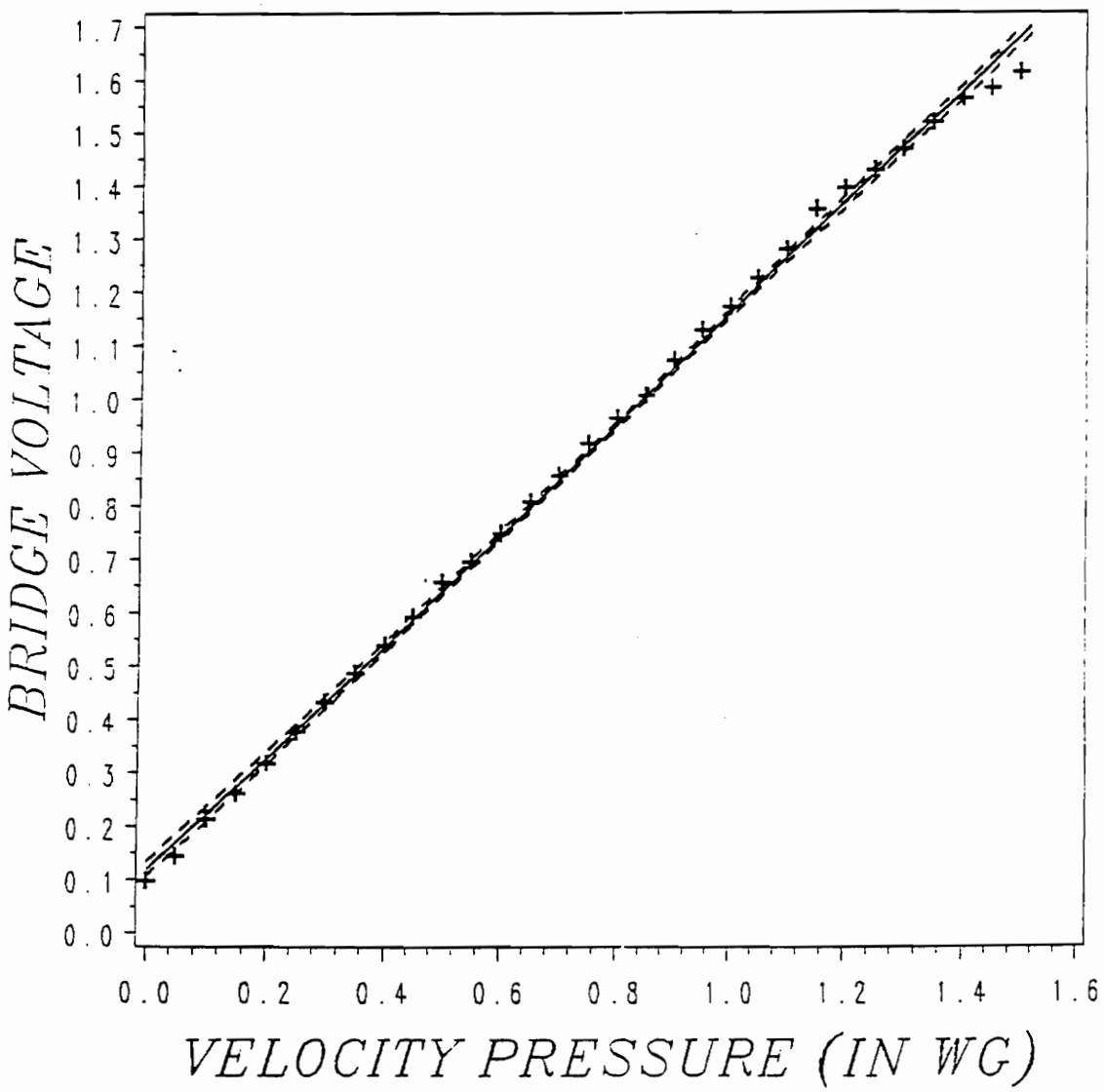

Figure 3.9 — Calibration Curve - WMS 1, Bolt Direction

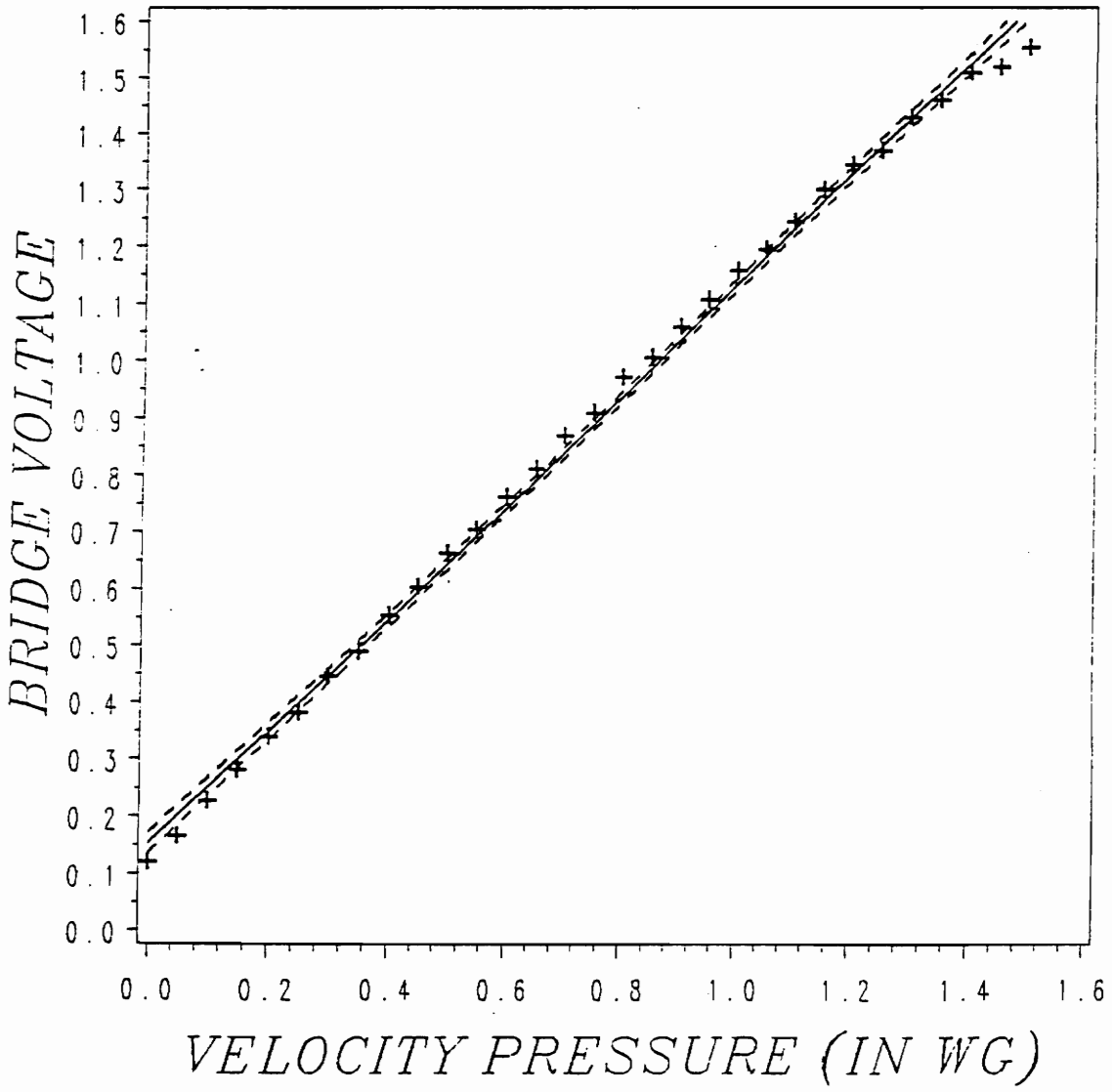

Figure 3.10 — Calibration Curve - WMS 1, Crosswise Direction

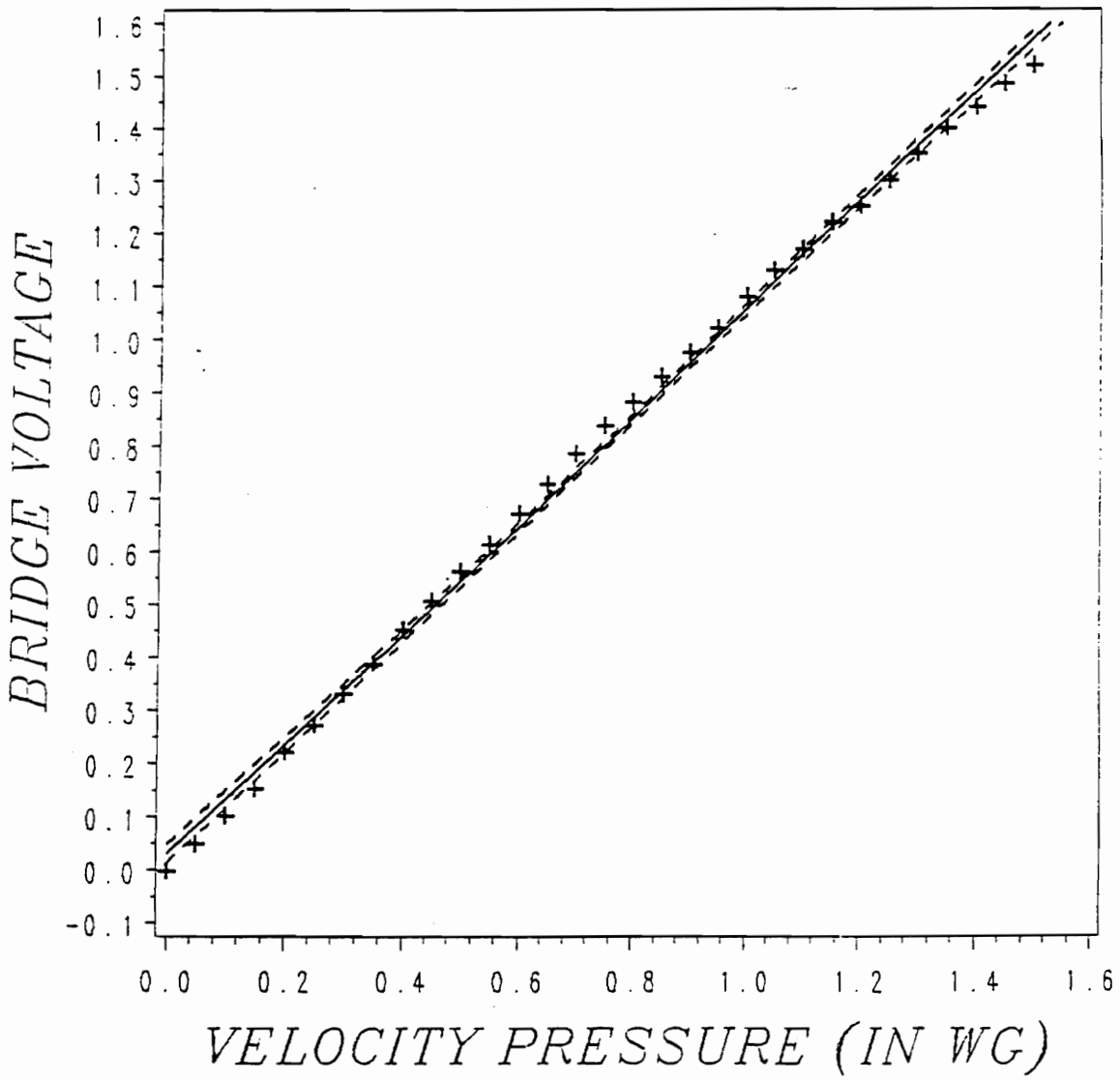

Figure 3.11 — Calibration Curve - WMS 2, Bolt Direction

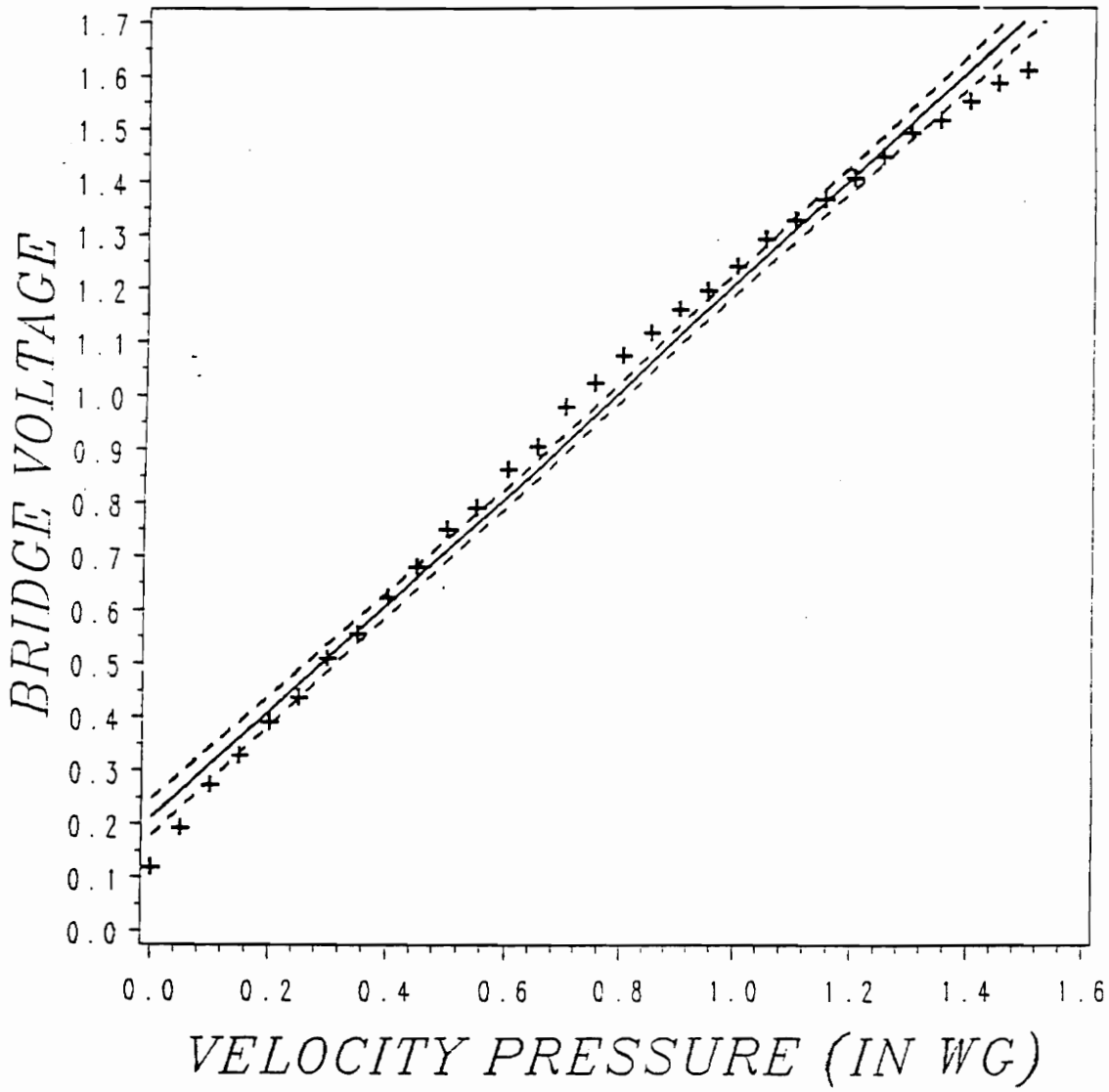

Figure 3.12 — Calibration Curve - WMS 2, Crosswise Direction

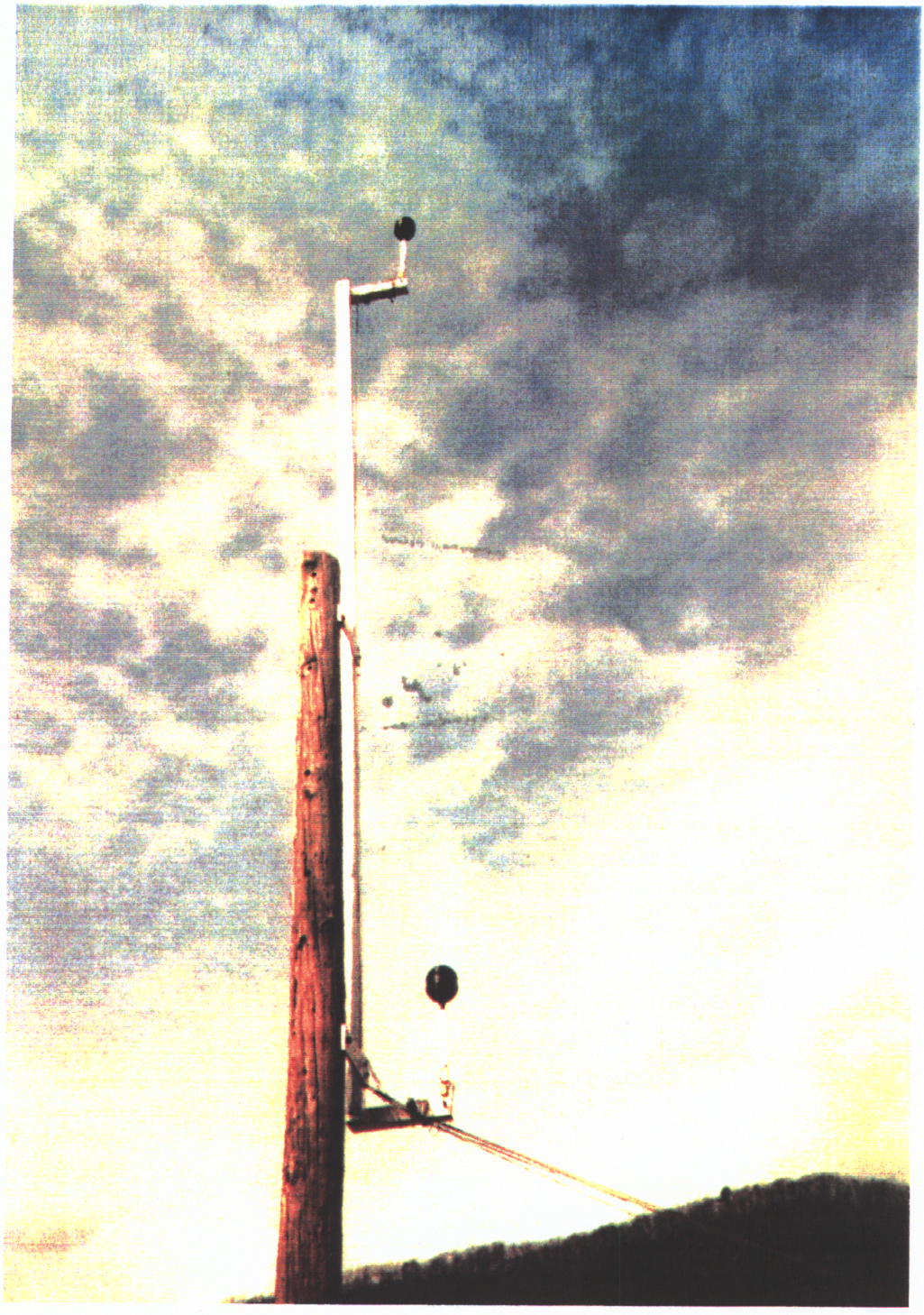

Figure 3.13 — View of Original Wind Measuring System

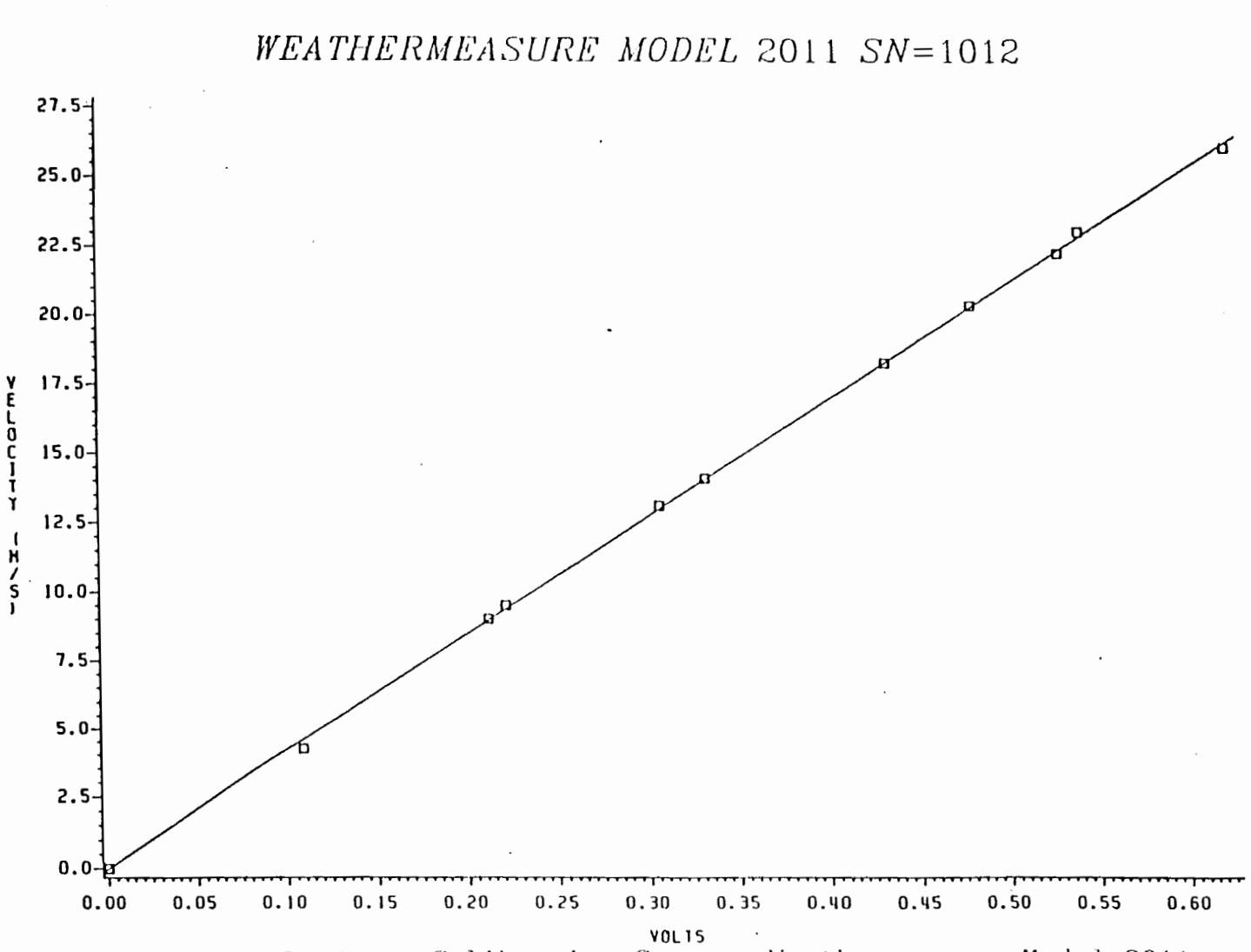

Figure 3.14 -- Calibration Curve - Weathermeasure Model 2011 Three Cup Anemometer

(Taken from reference 13)

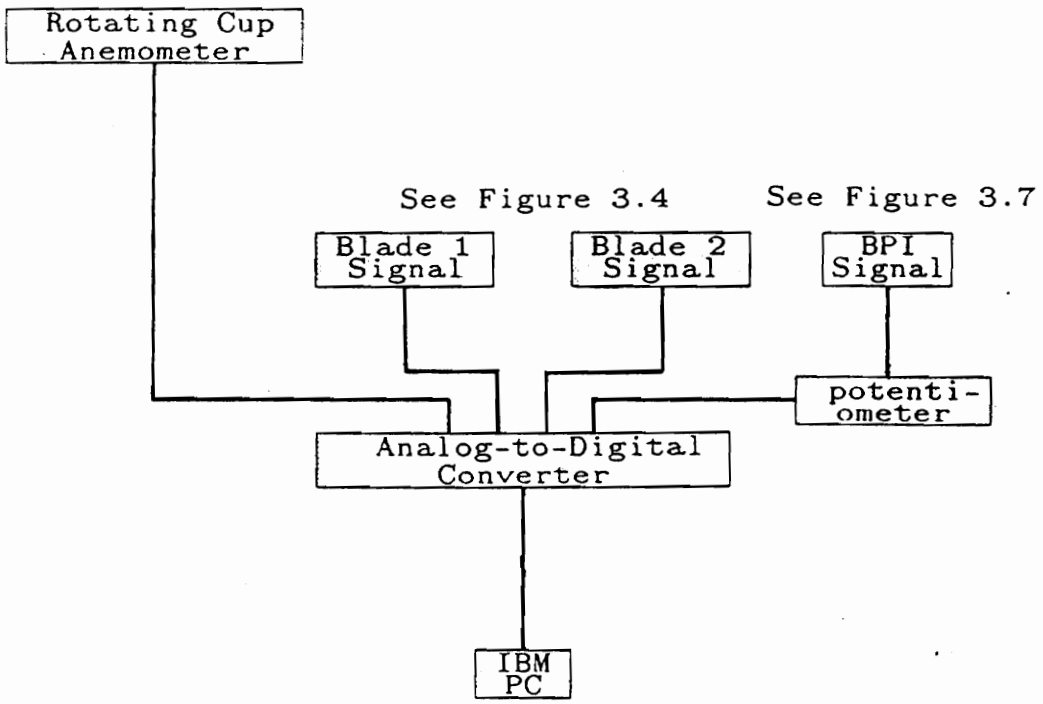

Figure 3.15 — Data Acquisition System Schematic

Table 3.1 — Control System Wiring Diagram Legend

SAB	Control Switch Limiter
SSp	Voltage Limiter
c	Capacitor
R_j	Resistor
R_{pot}	Potentiometer
SpKP	Voltage Control Potentiometer
ES	Brake Limit Switch
SM	Control Motor
SCH	Sliprings
VMS	Voltmeter Selector Switch
S_I	Fuse
V	Voltmeter
A	Ammeter
MK	Ground Terminal
o	Insulated Terminal
3	Hot Terminal
4	Stop Circuit Lead
8	Start Circuit Lead
SJB	Starting Relay
R,S,T	3-Phase Leads
F	Field Winding
ZL	Zener Diode Switch

Table 3.2 — Calibration Points - Blades 1 and 2

M (ft-lbf)	Blade 1 (V)	Blade 2 (V)
0.0	1.366	0.203
6.5	1.432	0.260
13.0	1.498	0.310
19.5	1.551	0.361
26.0	1.613	0.413
32.5	1.674	0.462
39.0	1.736	0.513
45.5	1.794	0.563

where M = Wind-Induced Bending Moment

Blade 1 = Bridge Voltage for Blade 1

Blade 2 = Bridge Voltage for Blade 2

Table 3.3 — Calibration Points - Wind Measuring System

P_V (in wg)	WMS1B (V)	WMS1X (V)	WMS2B (V)	WMS2X (V)
0.00	0.099	0.120	0.002	0.120
0.05	0.144	0.168	0.050	0.194
0.10	0.215	0.228	0.102	0.274
0.15	0.262	0.283	0.153	0.328
0.20	0.319	0.341	0.222	0.391
0.25	0.378	0.384	0.273	0.438
0.30	0.434	0.448	0.332	0.511
0.35	0.487	0.491	0.389	0.556
0.40	0.541	0.555	0.453	0.625
0.45	0.593	0.605	0.508	0.680
0.50	0.657	0.664	0.564	0.751
0.55	0.696	0.706	0.614	0.791
0.60	0.749	0.763	0.673	0.863
0.65	0.809	0.812	0.728	0.905
0.70	0.858	0.870	0.785	0.979
0.75	0.917	0.910	0.838	1.023
0.80	0.965	0.972	0.883	1.073
0.85	1.006	1.008	0.930	1.115
0.90	1.074	1.060	0.975	1.160
0.95	1.130	1.108	1.020	1.195
1.00	1.173	1.159	1.080	1.240
1.05	1.227	1.195	1.130	1.290
1.10	1.280	1.245	1.170	1.325
1.15	1.355	1.300	1.220	1.365
1.20	1.395	1.345	1.250	1.405
1.25	1.430	1.370	1.300	1.445
1.30	1.470	1.430	1.350	1.490
1.35	1.520	1.460	1.400	1.515
1.40	1.565	1.510	1.440	1.550
1.45	1.585	1.520	1.485	1.585
1.50	1.615	1.555	1.520	1.610

where P_V = Velocity Pressure

WMS1B = Bridge Voltage for WMS 1, Bolt Direction

WMS1X = Bridge Voltage for WMS 1, Crosswise Direction

WMS2B = Bridge Voltage for WMS 2, Bolt Direction

WMS2X = Bridge Voltage for WMS 2, Crosswise Direction

Table 3.4 — Data Acquisition System Channels

Channel	Function
0	Blade Position Indicator
1	Bridge Voltage - Blade 1
2	Bridge Voltage - Blade 2
3	Anemometer Output Voltage

CHAPTER 4 – RESULTS AND DISCUSSION

The data taken in this experiment consist of three elements: blade position, blade bending moment, and wind speed. The blade position indicator (BPI) worked well throughout the experiment, though the voltage output needed to be stepped down into the range of the analog-to-digital converter (ADC). As originally desired, the bending moment data of two blades were to be taken and compared; however, the instrumentation for blade 2 failed during the course of post-setup testing. Since data for only one blade are essential for the purposes of this experiment, it was decided to forego the difficult and time-consuming task of repairing the faulty instrumentation on the second blade. All bending moment data presented here, therefore, are taken from blade 1.

The wind measuring system (WMS) also presented severe problems. The very low level signals transmitted from the WMS assemblies to the strain indicators picked up large quantities of power line noise. The combined signal/noise combination could not be deciphered nor the desired information extracted. Efforts to eliminate the noise centered around grounding the WMS instrumentation such that

any line noise picked up would be conducted to the earth and thus would not interfere with the desired signals. In the order in which they were attempted they were:

1) Grounding the strain indicators and amplifiers to the WMS support structure,

2) Grounding the strain indicators and amplifiers to the ground spike,

3) Wrapping the low level signal wires with aluminum foil and grounding the foil to the grounding spike,

4) Moving the indicators and amplifiers as near the WMS assemblies as possible so as to have the long lead wires to the ADC at an amplified level.

None of the above-mentioned procedures resulted in a noticeable improvement in the signal-to-noise ratio, and the wind speed data remained severely contaminated.

Since blade bending moment data are essentially meaningless without corresponding wind speed data, an alternative WMS had to be employed. A Weathermeasure Model 2011 three-cup anemometer was mounted atop the shack at roughly the same height as the lower WMS assembly originally used. Some assessment of wind shear needed to be made, but with only one anemometer employed, determination of the upper level wind speed had to be determined theoretically. Shefter [26] presents a two-

dimensional approximation of the mean wind speed in the atmospheric boundary layer (ABL) of the form

$$v = v_1 \times \left[\frac{\lg(h/h_0)}{\lg(h_1/h_0)}\right]$$

where v is the wind speed at the desired height, h, v_1 is the known wind speed at height h_1, and h_0 is a height relating the roughness of the surface over which the wind must pass. A value of 1.3 in. (3.2 cm) is recommended for a surface covered by low grass, a condition present at the site. All of the data sets were taken with the wind blowing up the hill, thus free of obstructions other than low grass. The original WMS assemblies are at heights of 29 ft (8.8 m) and 15 ft (4.6 m), which correspond to the mean radius of the rotor. Since the anemometer is located at the same height as the lower WMS assembly, wind speed data for the upper WMS assembly were determined. Substituting the above heights results in

$$v = v_1 \times 1.13$$

It should be reiterated that the resulting value of upper level wind speed is an approximation, albeit a good one according to Shefter. The wind speed plots display both

the measured lower wind speed and the calculated upper wind speed.

Figures 4.1 - 4.10 display the blade bending moment and wind speed data collected for five separate data sets. Each data set has two plots, one for bending moment followed by one for wind speed. Each bending moment plot contains not only the bending moment data, but also the BPI pulse for use as an angular position reference. The transition from high to low in the pulse train indicates a blade position of 9:00 o'clock when looking downwind at the rotor.

Since no method of balancing the blade bridges exists, the DC offset must be determined in order to separate the bending-induced voltage from the offset. Also, an accounting of the magnitude of the gravity effect is desirable. Figure 4.11, taken the day of data acquisition, is a strip chart recording of one revolution of the rotor in a no-wind condition starting with blade 1 pointing straight down. The DC offset is taken at this position since no bending occurs, and its value is 1.6 V. The maximum deflection from the offset is roughly 100 mV, which translates to a maximum gravity-induced bending moment of 11 ft-lbf (15 m-N). The upper trace is the BPI signal,

while the lower trace displays the signal from blade 1.

It is evident that there is a large fluctuating bending moment with a frequency of one per revolution present as the blade travels around each revolution. Two effects cause this pattern. First, the difference in wind speeds at different heights, or wind shear, tends to cause higher moments while the blade travels through the uppermost section of its path. Second, gravity bends the blade in a periodic manner as the blade moves around its path. Also evident in most of the data is the blade natural frequency of about 6 Hz.

The moment reaches its maximum value when the blade is horizontal and moving down (the 3:00 o'clock position) and its minimum value when the blade is horizontal and moving up (the 9:00 o'clock position). These optima occur because the gravity-induced moment adds to the wind-induced moment at the former position and subtracts at the latter position as shown in Figure 4.12. The wind load tends to bend the blade back toward the tail at any given angular position, but the gravity load tends to bend the blade forward as the blade travels upward.

The maximum gravity-induced bending moment amplitude of 11 ft-lbf (15 m-N) is seen to account for the majority

of the fluctuation in the bending moment. Thus, only a small fraction of the bending moment's large fluctuation can be attributed to wind shear. The small size of this turbine precluded a large wind shear effect, though the large turbines used for commercial power generation should exhibit a significant effect as the difference in wind speeds between the upper and lower portions of the blade circle will tend to be greater.

The wind data were generally taken during gusty periods. In general, the air was calm except for periodic wind gusts, during which data were collected. Some of the wind data exhibit a fairly constant overall mean speed, though in the rest of the data the end of the wind gust can be noted by the steady decline in wind speed. A dominant frequency of about 3 Hz is evident in all of the wind data, possibly due to a characteristic harmonic of the WM-2011 anemometer. Nevertheless, the variation of the mean wind speed is easily discernible.

In order to judge the accuracy of the ABL approximation to these particular data sets, it is noted that the bending moment is proportional to the square of the wind speed. Thus if the difference in wind speeds is 13%, as predicted by the ABL approximation for vertical

shear, then the difference in bending moments should be on the order of 28%. The bending moment plots were examined, and Table 4.1 was generated. Values are tabulated for each complete cycle in the sampling period for each data set. No results for data set 1 are available since one complete revolution did not occur in the sampling period. The bending moment ratio (BMR) indicated is that between the 12:00 position and the subsequent 6:00 position for a given cycle. The BMR as predicted should be 1.28, while the measured average is 1.33 for all of the data sets, which yields a +3.9% deviation. Large variations from the mean exist for some cycles, however, indicating that the ABL approximation holds fairly well in the mean, but cannot account for random fluctuations in the wind shear profile. A point to keep in mind here is that in reality the BMR is proportional to the relative velocity of the wind to the blade, thus the above results are approximate though encouraging. The relative velocity depends upon both the wind speed and the rotational speed of the rotor, which may not be constant at a given wind speed.

It is evident that the rotor speed varies considerably between data sets even though the differences in wind speeds are relatively minor. The reason for this

discrepancy is the fact that the rotor's inertia requires time for the rotor to respond to changes in wind speed. Thus, if the data indicate a rotor speed lower than expected for a given wind speed, it is because the rotor had not yet come up to speed during the sampling period.

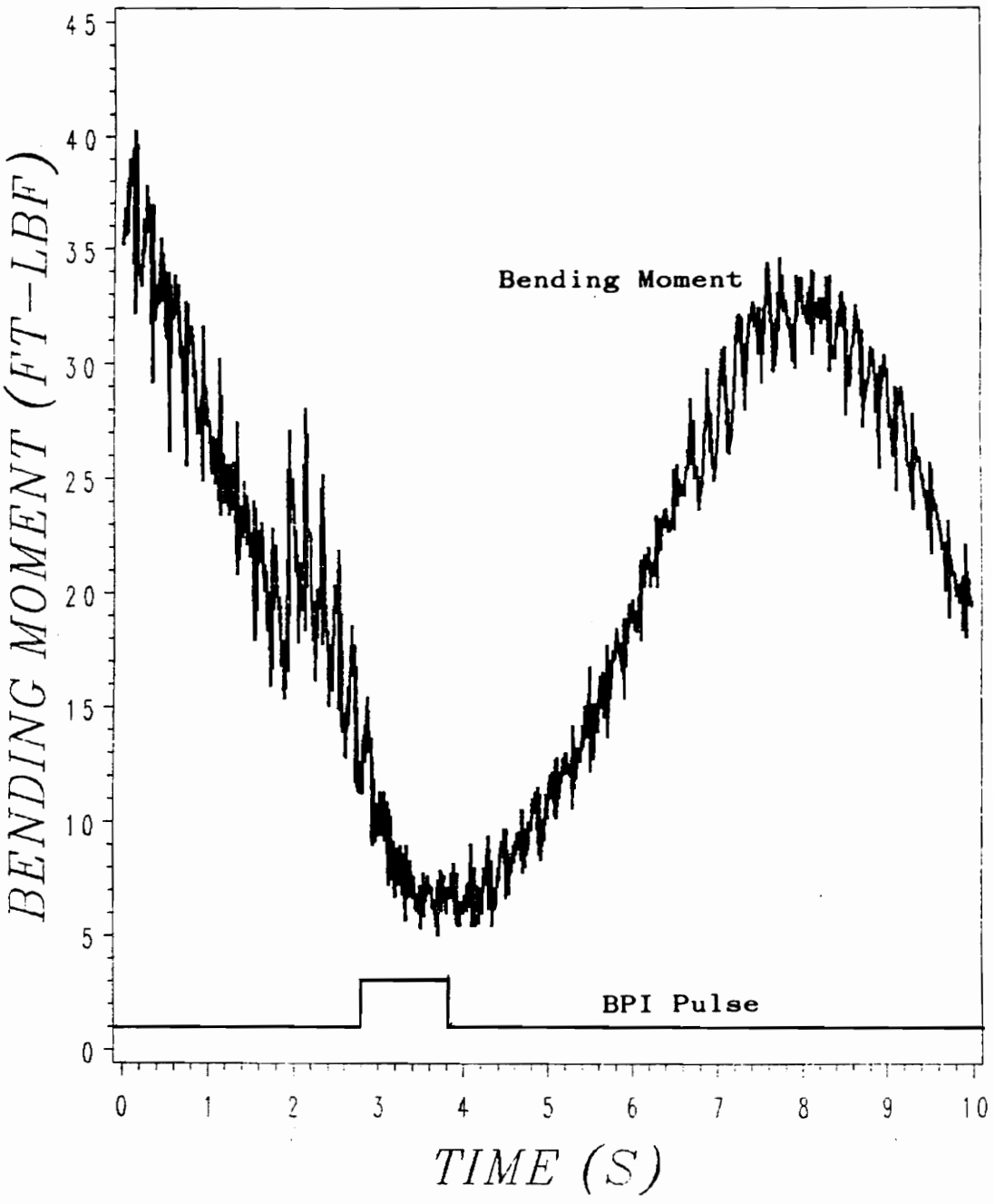

Figure 4.1 — Blade Bending Moment - Data Set 1

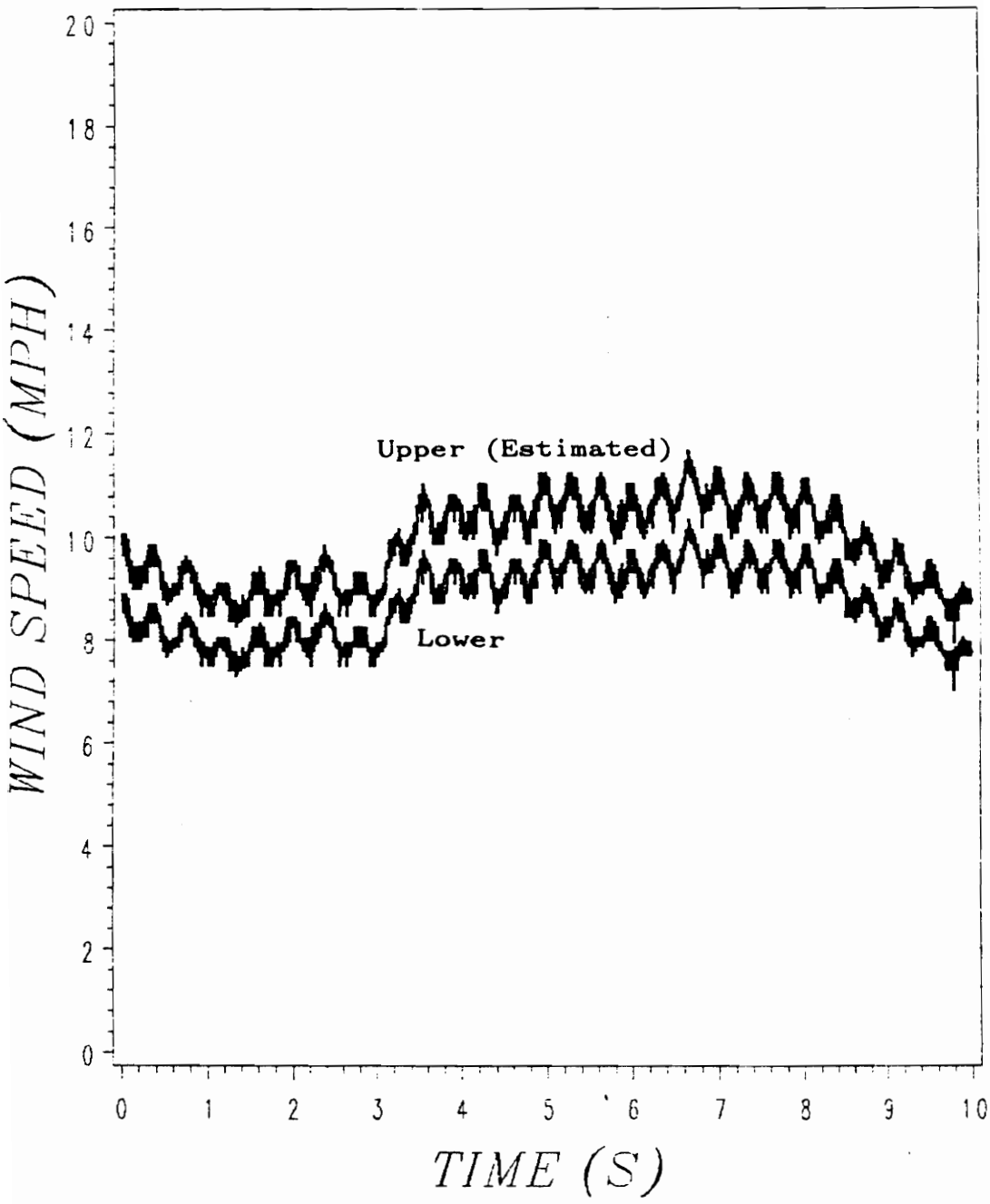

Figure 4.2 — Wind Speed - Data Set 1

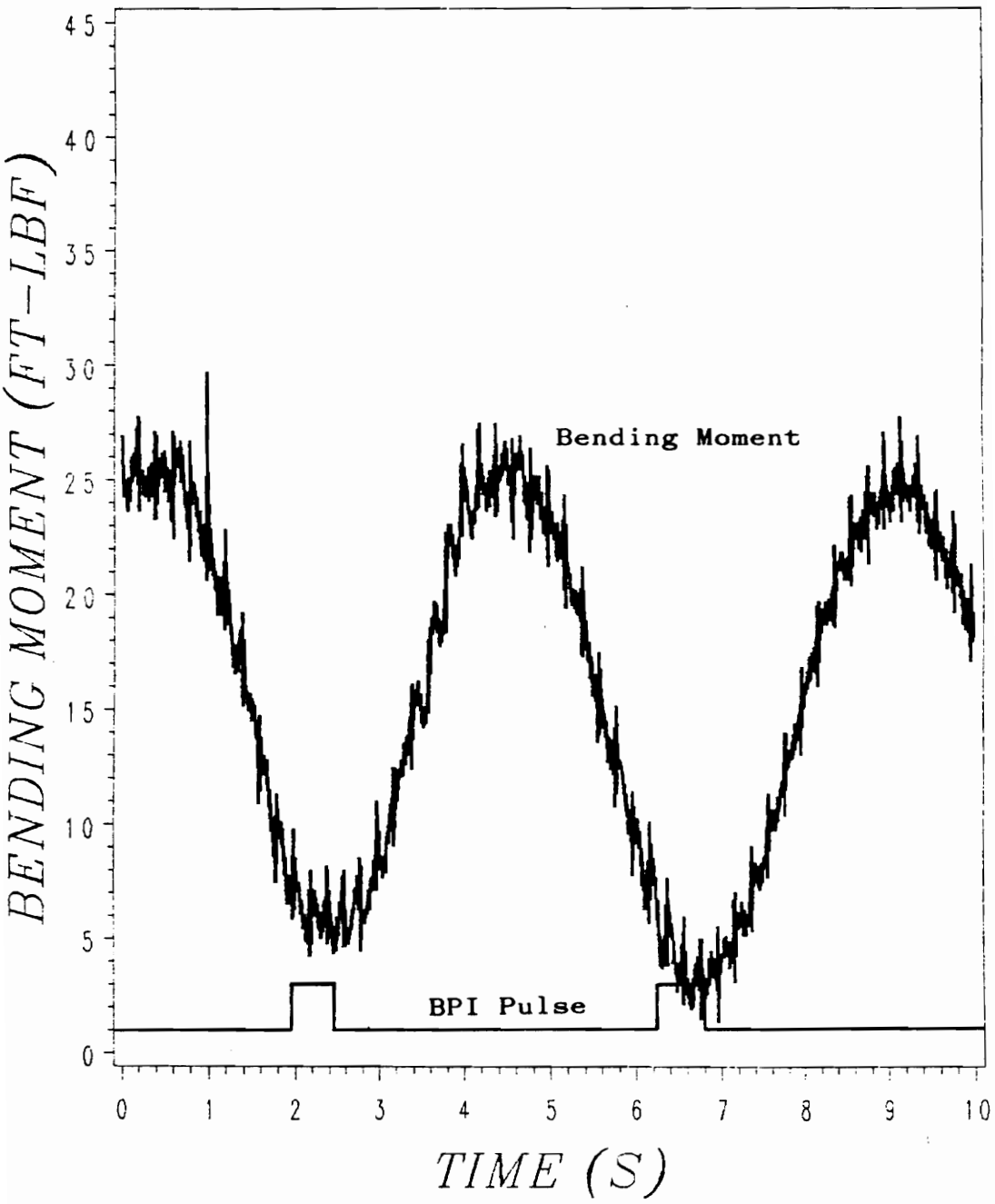

Figure 4.3 — Blade Bending Moment - Data Set 2

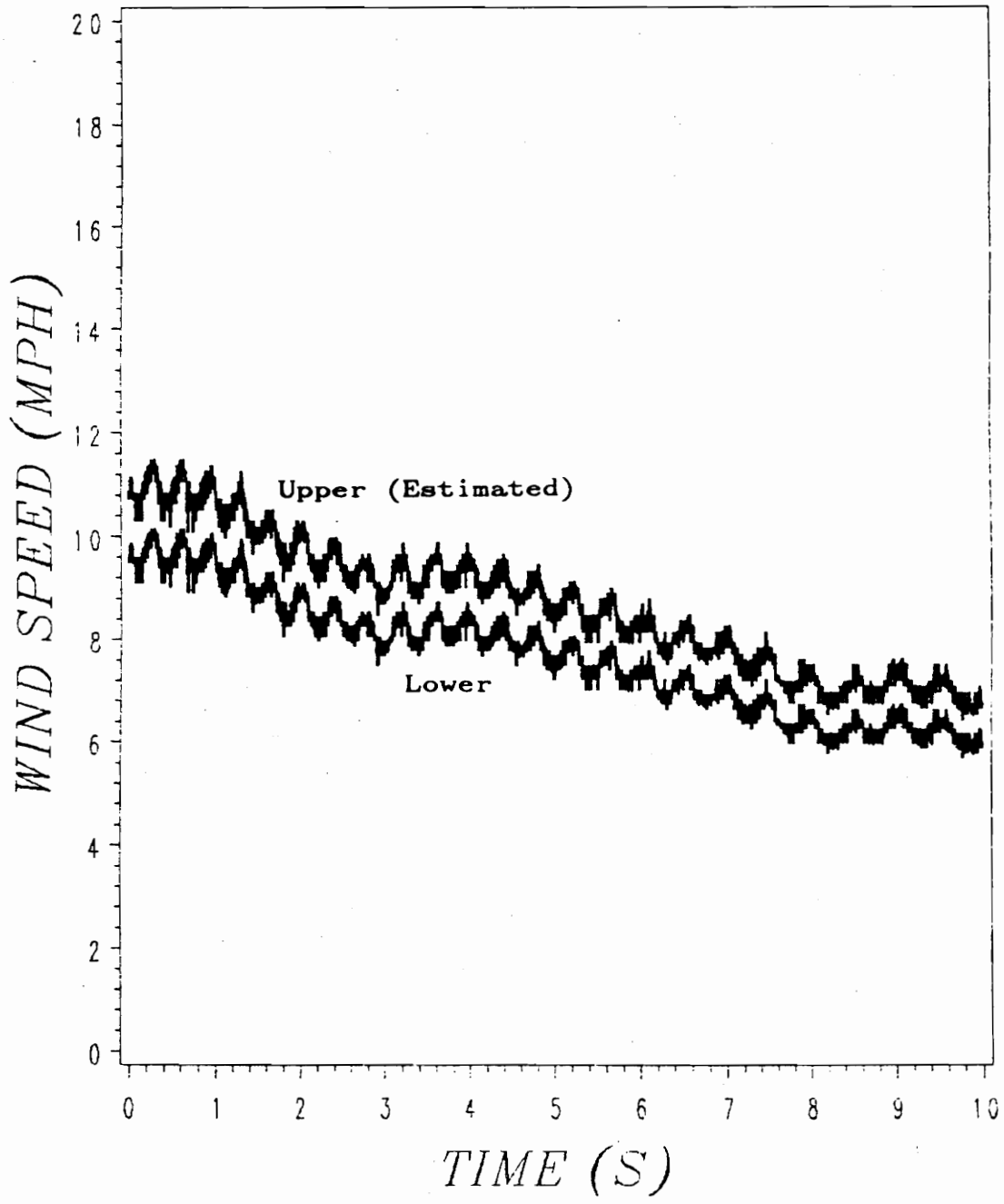

Figure 4.4 — Wind Speed - Data Set 2

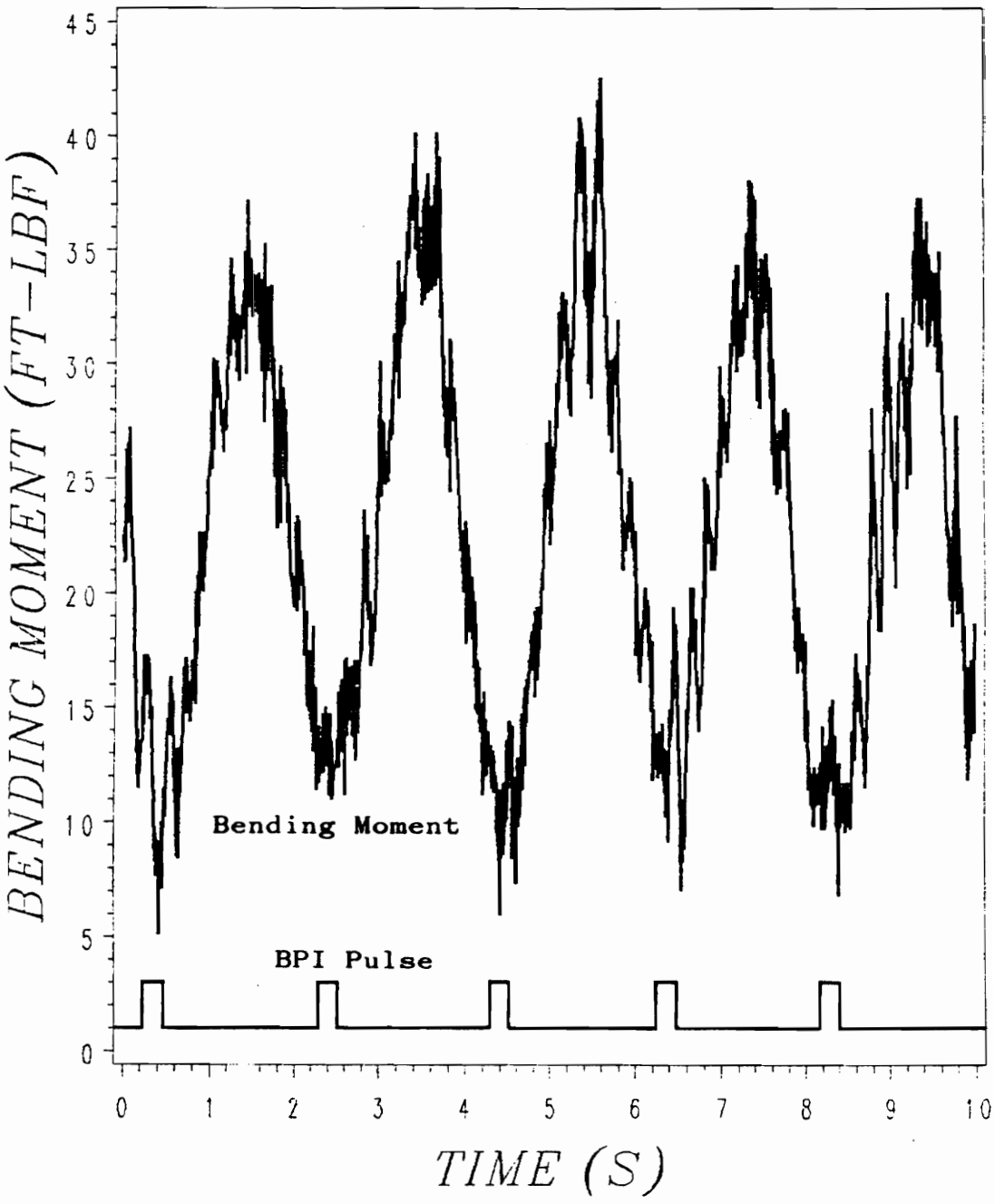

Figure 4.5 — Blade Bending Moment - Data Set 3

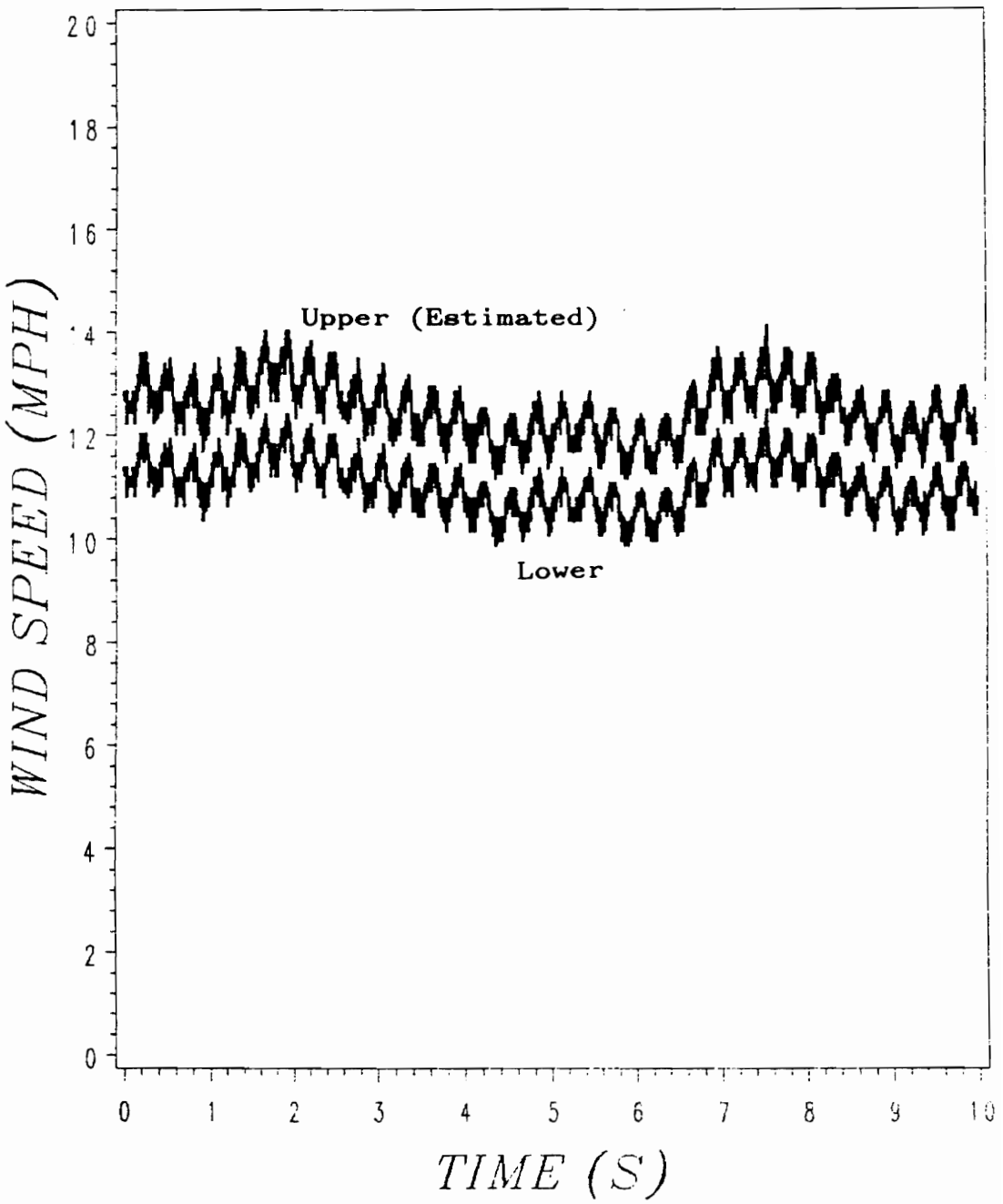

Figure 4.6 — Wind Speed - Data Set 3

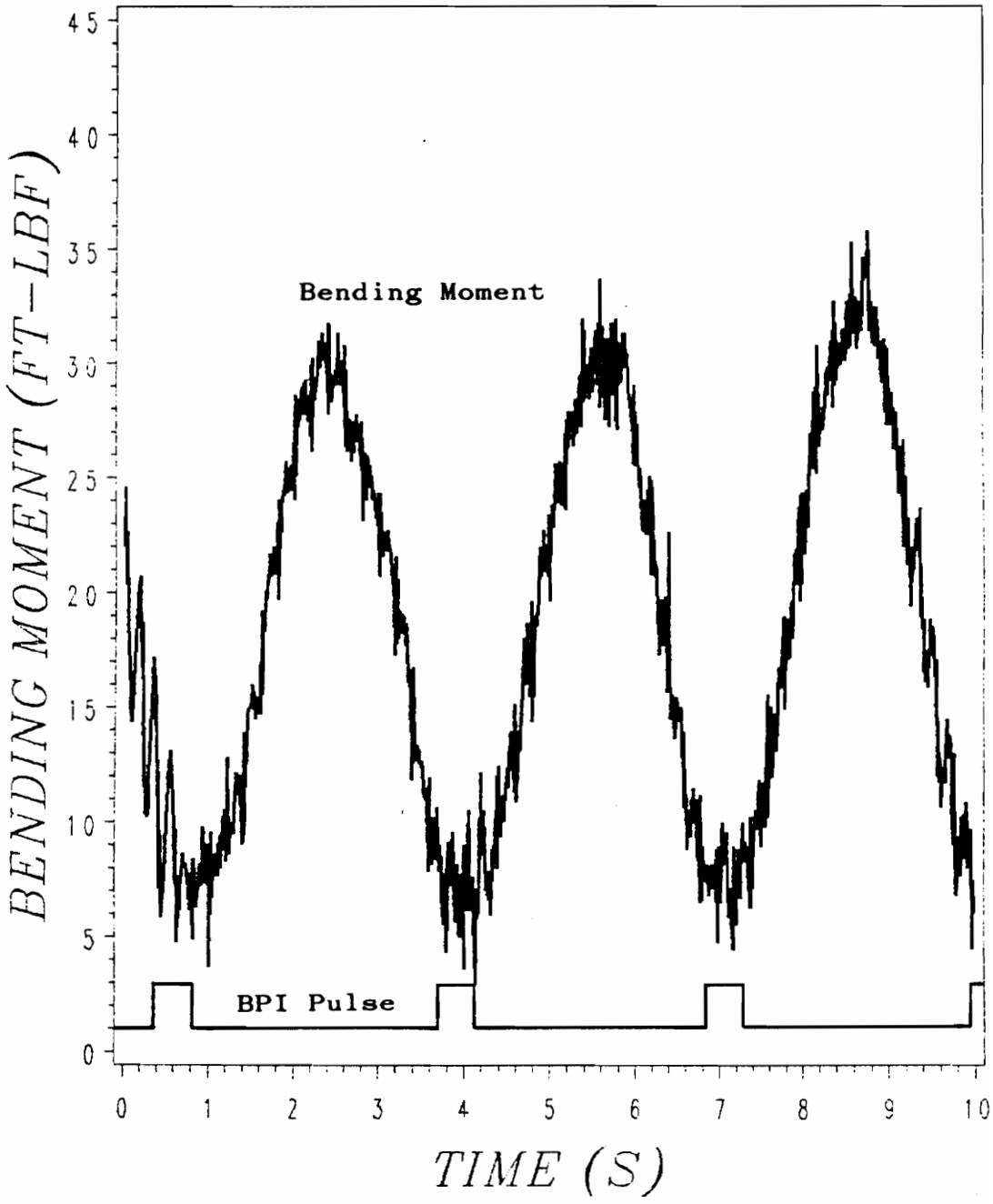

Figure 4.7 — Blade Bending Moment - Data Set 4

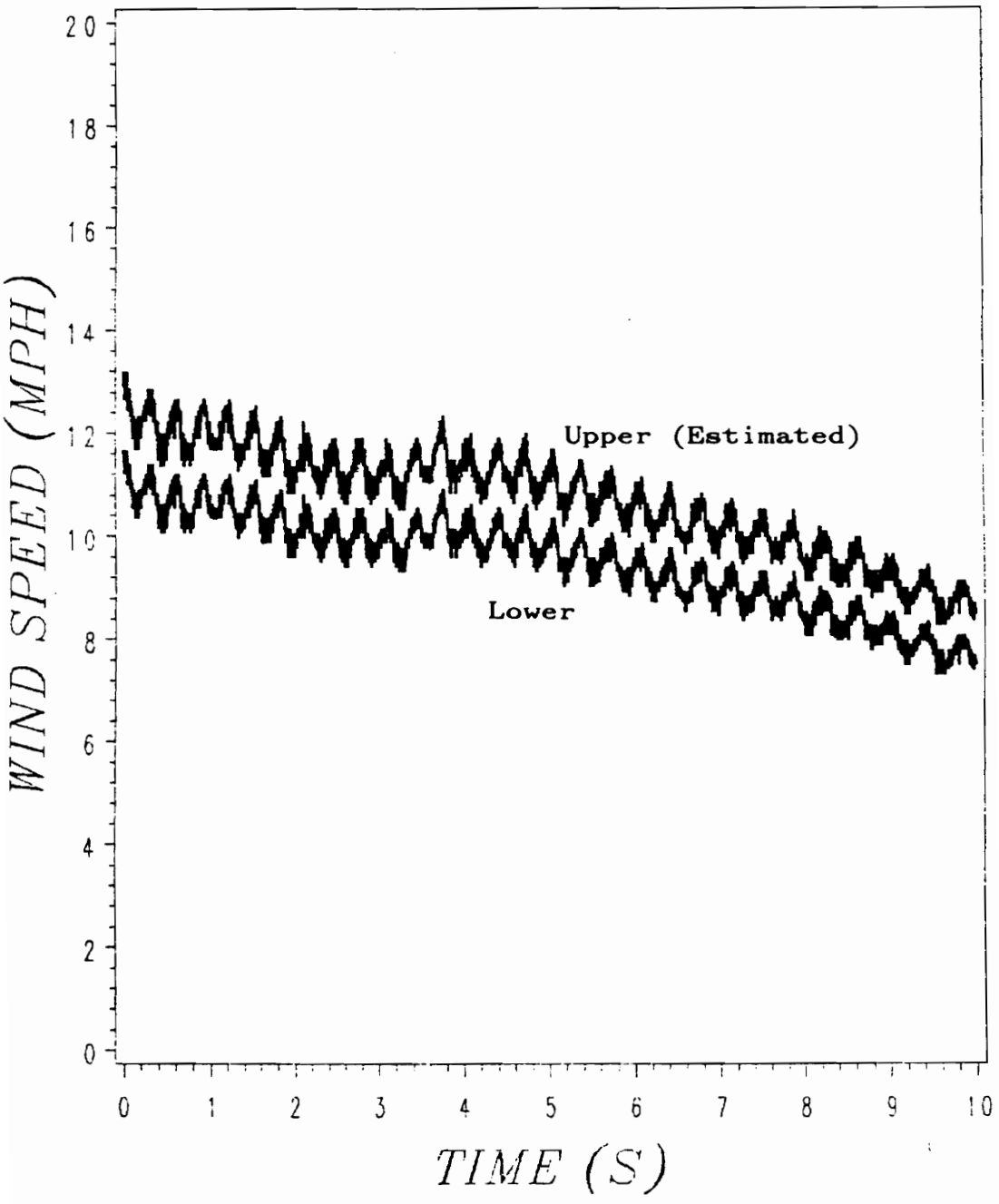

Figure 4.8 — Wind Speed - Data Set 4

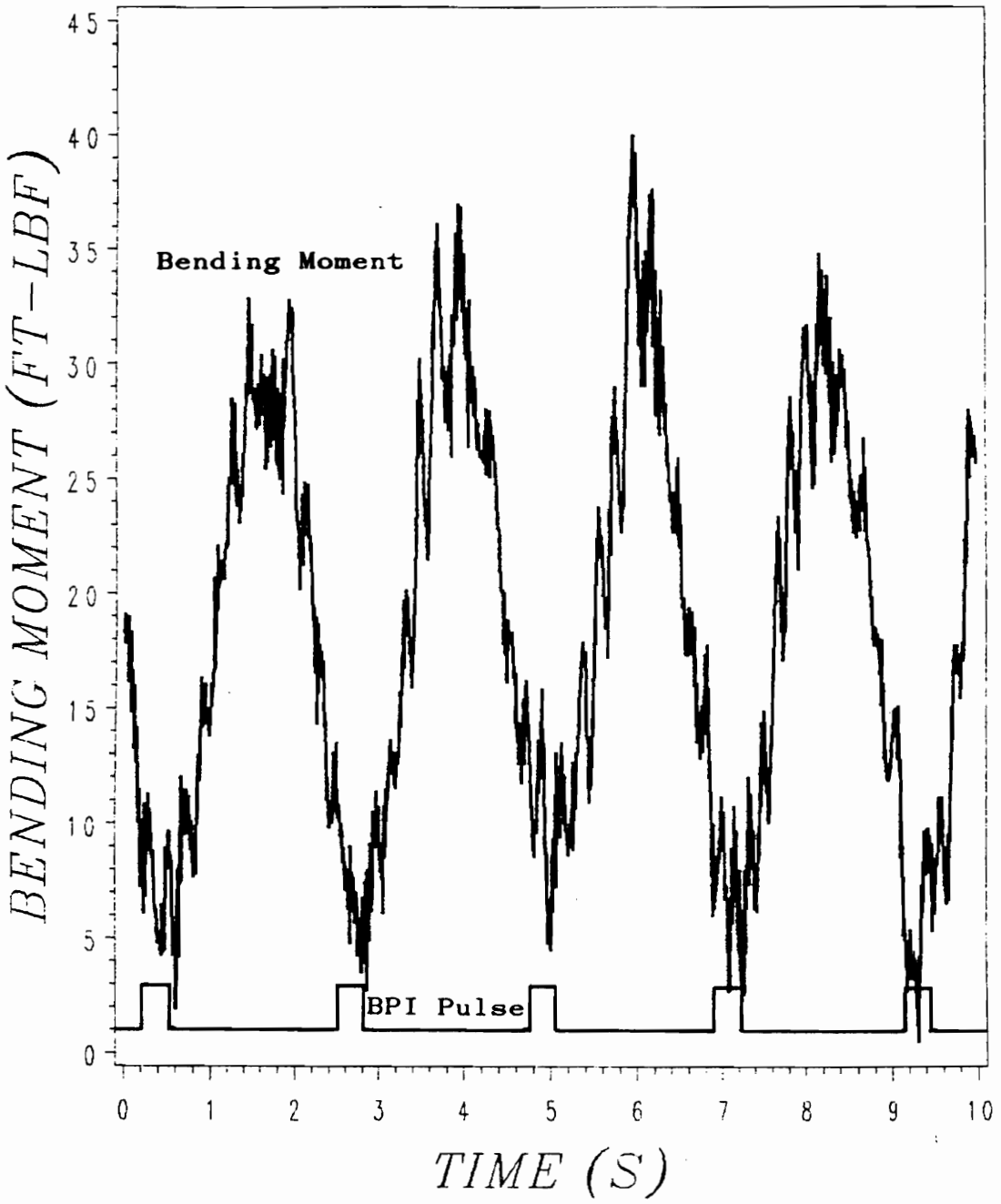

Figure 4.9 — Blade Bending Moment - Data Set 5

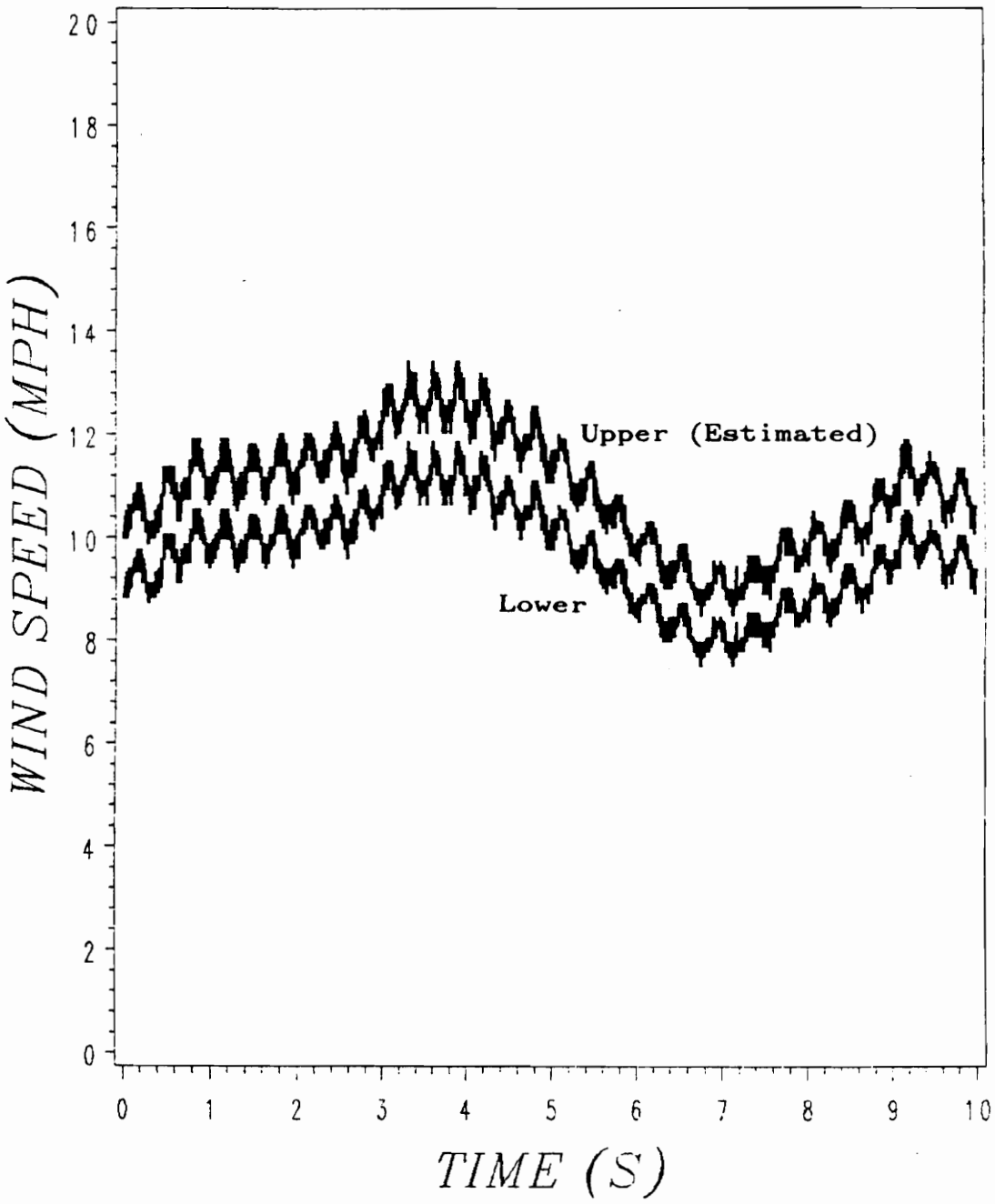

Figure 4.10 — Wind Speed - Data Set 5

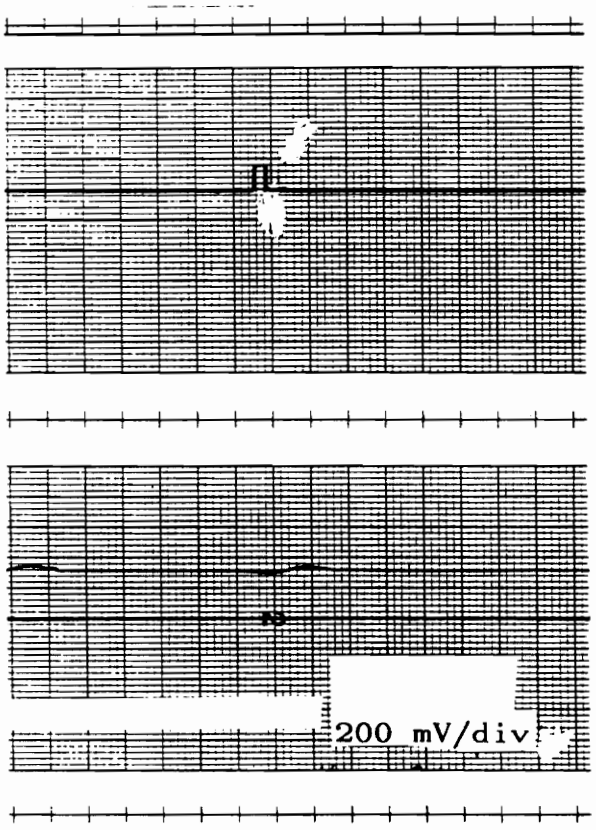

Figure 4.11 — BPI Pulse and Blade 1 Voltage, One Rotation with No Wind

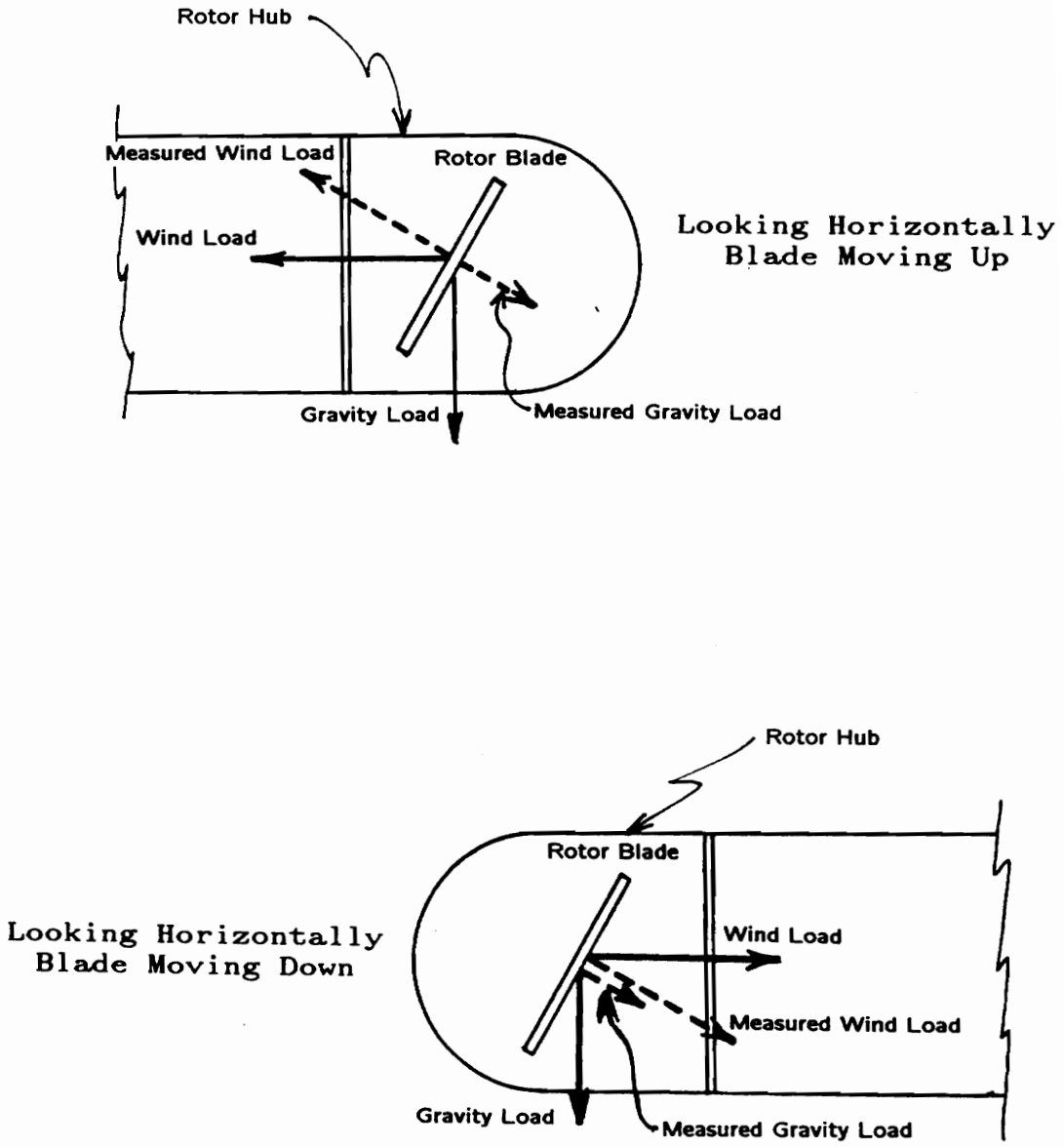

Figure 4.12 — Effect of Gravity-Induced Bending Moment

Table 4.1

Bending Moment Ratios Between 12:00 and 6:00 Positions

Data Set	Bending Moment (ft-lbf) Position 12:00	6:00	Bend. Mom. Ratio	% Dev. from ABL approx.
1	*	*	*	*
2	17	13.5	1.26	-1.6
3	25	20.5	1.22	-4.7
	25.5	20	1.28	0.0
	26	17.5	1.48	15.6
	25	17	1.47	14.8
4	19	18.5	1.03	19.5
	21.5	15	1.43	11.7
5	21	17	1.24	-3.1
	18.5	16	1.15	10.2
	20.5	14	1.46	14.1
	24	15	1.60	25.0

Average Bending Moment Ratio : 1.33
Average % Deviation from ABL Approx. : +3.9

* — Indicates one complete cycle not acquired

CHAPTER 5 – CONCLUSIONS AND RECOMMENDATIONS

CONCLUSIONS:

1) Data have been obtained for the in-plane moment as a function of angular position and wind velocity for a small HAWT.

2) Large one-per revolution fluctuations in bending moment are evident due mainly to gravity at low wind speeds. At high wind speeds, fluctuations due to wind shear would be predominant.

3) The ratio of bending moment due to wind shear between the 6 o'clock and 12 o'clock positions is approximately 1.33. This would be significant in estimating fatigue.

4) An approximation of the atmospheric boundary layer gives a reasonable estimate of the brnding moment fluctuation due to wind shear.

RECOMMENDATIONS:

The recommendations are divided into two sections, one dealing with improvements to the present work, the other suggesting future studies involving this wind turbine.

I. IMPROVEMENTS TO PRESENT WORK

1) Discontinue use of the strain indicators and amplifiers employed with the drag sphere anemometers and build compact, complete bridge/amplifier circuits on the WMS pole itself to eliminate low voltage level signal transmission to the data acquisition system.

2) Repair the on-rotor instrumentation for blade 2 to allow a comparison study to be performed between the two blades.

II. FUTURE STUDIES

3) Perform a fatigue analysis on the blades. This could be performed with the present data, though some fluctuations may have been too rapid to be detected with the equipment used here. Use of the drag sphere anemometers, if operational, is advised.

4) Instrument the blades to detect pressure variations across the blade surfaces to facilitate a thorough

aerodynamic study of the blades.

5) Measure tower loads to determine thrust and yaw characteristics of the turbine. These figures could be compared to those generated by prediction codes.

REFERENCES

1. Solar Energy Research Institute, Wind Energy Technical Information Guide, December, 1989.

2. Torrey, V., Wind-Catchers, American Windmills of Yesterday and Tomorrow, Stephen Greene Press, Brattleboro, Vermont, 1976.

3. Golding, E. W., The Generation of Electricity by Wind Power, John Wiley & Sons, Inc., New York, New York, 1977.

4. Figard, R. L., "The Aerodynamic Analysis of a 10 kW Horizontal Axis Windmill", Doctoral Dissertation, VPI&SU, 1980.

5. Koeppl, G. W., Putnam's Power from the Wind, 2d. ed., Van Nostrand Reinhold Co., New York, New York, 1982.

6. Schetz, J. A., O'Brien, W., Tanchoco, J., Vaughan, D. and Wysk, R., "Application of Windmills to Apple Cooling and Storage", SEA Contract 12-14-1001-960, VPI&SU, 1981.

7. Benim, T. E., "Performance Measurement of a Ten Kilowatt Horizontal Axis Wind Turbine", Master's Thesis, VPI&SU, 1977.

8. Hinerman, J. M., Jr., "Performance Measurement and Optimization of an Upwind-Rotor, Horizontal-Axis Wind Turbine at Various Yaw Angles", Master's Thesis, VPI&SU, 1979.

9. Moses, H. L. and Hawkins, L. E., "Final Report: Environmental Effects on Wind Turbines", Mechanical Engineering Department, VPI&SU, 1987.

10. Snow, A. L., Heberling, C. F. II and Van Bibber, L. E., "The Dynamic Response of a 600-kW Wind Turbine", Westinghouse Electric Corporation, 1989.

11. Osgood, R. M. and Coleman, C., "A Comparison of Rigid Hub and Teetering Hub Operating Loads for the Northern Power 100-kW Wind Turbine", AWEA Windpower '89.

12. Wright, A. D. and Thresher, R. W., "Prediction of Stochastic Blade Responses Using Measured Wind-Speed Data as Input to the FLAP Code", Journal of Solar Energy Engineerng, November 1990.

13. Wright, A D., Weber, T. L., Thresher, R. W., and Butterfield, C. P., "Prediction of Stochastic Blade Loads for Three-Bladed, Rigid-Hub Rotors", Ninth ASME Wind Energy Symposium, January 1990.

14. Hansen, A. C., Butterfield, C. P., and Cui, X., "Yaw Loads and Motions of a Horizontal Axis Wind Turbine", Transactions of the ASME, November, 1990.

15 Hansen, A. C. and Cui, X., "A Summary of Experiences in the Analysis of Rigid-Rotor Yaw Control Systems", presented at the Thirteenth Annual Energy-Sources Technology Conference and Exhibition, January, 1990.

16. Hansen, A. C. and Cui, X., "Analysis and Observations of Wind Turbine Yaw Dynamics", Journal of Solar Energy Engineering, November, 1989.

17. Mohamadian, H. P. and Graham, I. J., "Stiffness Degradation in Unidirectional and Chopped-Mat E-Glass Fiber/Polyester and Vinylester Composite Laminates", ASME Proceedings, January, 1991.

18. Graham, I. J. and Mohamadian, H. P., "Fatigue Testing of Unidirectional and Chopped-Mat E-Glass Fiber Polyester and Vinylester for Wind Turbine Blades", Proceedings Windpower '90, September, 1990.

19. Graham, I. J., Mohamadian, H. P., and Wang, C. S., "Fatigue Life Characteristics of E-Glass Fiber Reinforced Polyester and Polyvinylester Composites", Proceedings Windpower '89, September, 1989.

20. Bentley, J. P., Principles of Measurement Systems, 2d. ed., John Wiley and Sons, Inc., New York, 1988.

21. Thomson, W. T., Theory of Vibration with Applications, 3d. ed., Prentice Hall, Englewood Cliffs, New Jersey, 1988.

22. Shames, I. H., Mechanics of Fluids, 2d ed., McGraw-Hill Book Company, New York, New York, 1982.

23. Wilks Wells, K., Laboratory Notebook, VPI&SU, 1985.

24. Data Translation, Inc., LPCLAB, User Manual, Version V01.00. 1987.

25. Elektro, G.m.b.H., "Operating Manual for the WVG-120G", Winterthur, Switzerland, 1977.

26. Shefter, Y. I., Wind-Powered Machines, Leo Kanner Associates, Redwood City, California, 1974.

APPENDIX A

Original Specifications for the Elektro WVG-120G Wind Turbine

Original Specifications for the Elektro WVG-120G Wind Turbine*

Rated Power Output	10 kW
Output Voltage	110 V
Rated Windspeed	24 mph (10.7 m/s)
Number of Phases	3
Output Frequency Range	30-135 Hz
Output rpm Range	55-245 rpm
Propeller Diameter	21.7 ft (6.6 m)
Number of Blades	3
Field Regulation	Combination of 2 Permanent Magnets and 2 Field Rotor Sections
Field Current	1.2-1.5 A
Field Voltage	50-80 V
Field Power	60-120 W
Generator Weight	628 lb (285 kg)

*From reference 25.

VITA

David Gerard Hendricks was born on May 16, 1966 in Des Plaines, Illinois, just outside of Chicago. He spent his early childhood in New Orleans, Louisiana, and moved to Virginia Beach, Virginia, in 1975. He attended Princess Anne High School and was graduated in 1984.

He entered Virginia Tech in the fall of 1984 and participated in the Cooperative Education Program with Newport News Shipbuilding. He completed his Bachelor of Science degree in Mechanical Engineering in May, 1989. He continued his education at Virginia Tech and completed the requirements for his Master of Science degree in Mechanical Engineering in May, 1991.

His future plans include employment at the Brunswick Nuclear Plant of Carolina Power and Light Company south of Wilmington, North Carolina. He also plans to get married in November, 1991.

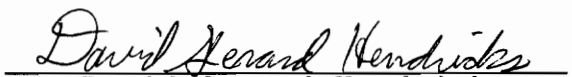

David Gerard Hendricks